



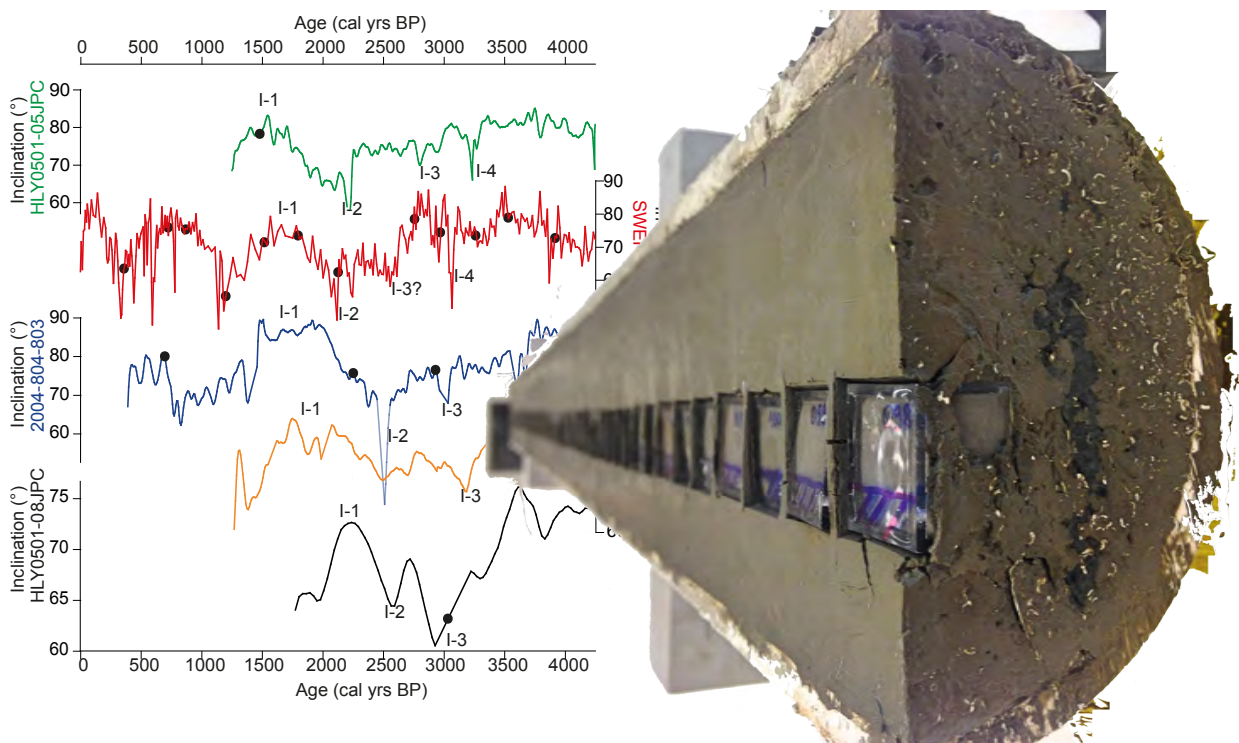
Stockholm University

Master Thesis

Degree Project in Marine Geology 60 hp

An independently dated 4200-year palaeomagnetic secular variation record from the Chukchi Sea, Arctic Ocean

Gabriel West



Stockholm 2017

Department of Geological Sciences
Stockholm University
SE-106 91 Stockholm

An independently dated 4200-yr palaeomagnetic secular variation record from the Chukchi Sea, Arctic Ocean

Developing highly-tuned and accurate age models for Arctic Ocean sediments has been a long-standing problem in marine geosciences. This problem stems from the often microfossil poor content of these sediments and low sedimentation rates away from continental margins. The absence of reliable chronologies limits our ability to interpret increasingly sophisticated proxies for past environmental changes in this sensitive ocean basin, and prevents the integration of Arctic palaeoceanographic time series with terrestrial, lacustrine and ice core records. While palaeomagnetism has the potential to help resolve this problem, there is a scarcity of independently dated records from the Arctic and an incomplete understanding of mechanisms by which sediments become magnetized. Recently published results from a few western Arctic Ocean sediments illustrate that patterns and variability in Holocene palaeosecular variation appear consistent with low latitude North American records and output from spherical harmonic geomagnetic field models. However, these marine records are constrained by only a few, and in some cases no, independent age data.

A detailed palaeo- and environmental magnetic record from an 8.24 m long sediment core (SWERUS-L2-2-PC1) collected at 57 m water depth in the Herald Canyon, Chukchi Sea of the Arctic Ocean (72.52° N 175.32° W) is presented. An independent age model for the core, which covers the last 4200 years, was derived from 14 AMS ¹⁴C dates and the identification of a tephra layer associated with the 3.6 cal ka BP Aniakchak eruption. The age model indicates average sedimentation rates of ~ 200 cm/kyr. Variability in the palaeomagnetic declination and inclination conform well to predictions made by time-varying geomagnetic field models (A_FM, pfm9k.1a, CALS3K.4e and CALS10k.1b) and can be readily correlated to other published PSV records from the Western Arctic that lack independent age control. The Late Holocene PSV record from SWERUS-L2-2-PC1 has the potential to be one of the best and most northerly reference curves for high latitude geomagnetic variability, and provide critical insights into the nature of geomagnetic field behaviour in the Arctic.

Table of Contents

1. INTRODUCTION	3
2. REGIONAL SETTING	7
3. AGE MODEL AND LITHOLOGY	9
4. MATERIALS AND METHODS	13
A. CORE DESCRIPTION AND SAMPLING PROCEDURE	13
B. PALAEOMAGNETIC MEASUREMENTS	14
<i>i. Magnetic susceptibility</i>	14
<i>ii. Natural remanent magnetisation (NRM)</i>	14
<i>iii. Anhyseretic remanent magnetisation (ARM)</i>	15
<i>iv. Isothermal remanent magnetisation (IRM)</i>	15
5. RESULTS.....	17
A. MAGNETIC SUSCEPTIBILITY AND ANISOTROPY OF MAGNETIC SUSCEPTIBILITY	17
B. NATURAL REMANENT MAGNETISATION AND PALAEOMAGNETIC DIRECTIONAL DATA	19
C. MAGNETIC GRAIN SIZE AND CONCENTRATION	23
D. RELATIVE PALAEOINTENSITY DETERMINATION	25
6. DISCUSSION	27
A. ANISOTROPY OF MAGNETIC SUSCEPTIBILITY	27
B. COMPARISON WITH GEOMAGNETIC FIELD MODEL OUTPUTS.....	28
C. COMPARISON WITH WESTERN ARCTIC PALAEOMAGNETIC RECORDS.....	32
D. FUTURE PERSPECTIVES	36
7. CONCLUSIONS.....	37
8. ACKNOWLEDGEMENTS	38
REFERENCES	39
APPENDICES.....	43
APPENDIX I.....	43
APPENDIX II.....	44
APPENDIX III.....	47

1. Introduction

Palaeomagnetism has played a key role in the advancement of geology over the centuries by providing essential evidence for theories such as plate tectonics and sea-floor spreading. The fundamental relationship between Earth's magnetic field and the magnetic properties of rocks and sediments allowed it to be used as a geochronological tool. Rocks and sediments are capable of recording characteristics of the ambient field at the time of their formation / deposition. However, deciphering the preserved magnetic signal is not without its challenges. This is particularly true for the magnetic record of sediments: the magnetisation process of which is not fully understood (Tauxe, 1993; Valet, 2003). Ocean currents during deposition, bioturbation, diagenetic processes, magnetisation prior to deposition can all distort this signal (Bradley, 2015).

Interpretation difficulties are further complicated by incomplete knowledge of the geomagnetic field behaviour, particularly at high latitudes. Earth's magnetic field is generated by a dynamo action produced by circulation of charged particles in the liquid outer core (Kearey, 2002). The outer core has different convective regimes, separated by a hypothetical tangent cylinder (Lawrence et al. 2009), which intersects the core-mantle boundary at around 69.5° latitudes, and the Earth's surface at 79° on both hemispheres (Figure 1). As a result, in the poleward regions bound by the latitudinal circles of approximately 70° the geomagnetic field is thought to have unique characteristics (St-Onge and Stoner, 2011; Lund et al. 2016).

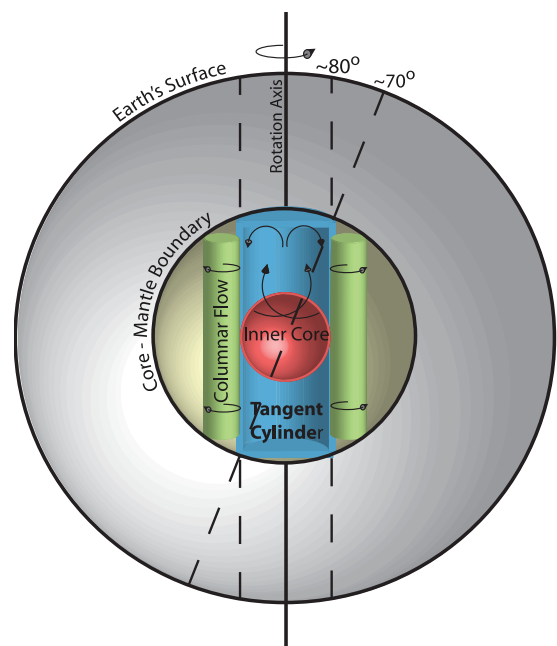


Figure 1: Illustration of the tangent cylinder and its surface expression (Lawrence et al. 2009).

The complexity of the magnetisation process of sediments coupled with a probable unique magnetic field behaviour at the Arctic led to controversial interpretations of Arctic Ocean palaeomagnetic records. Shallow, and negative magnetic inclinations were observed in sediment cores retrieved from the Arctic Ocean, and interpreted as polarity reversals, reflecting magnetic polarity chron changes (e.g. Clark et al. 1984). A significant shift in views on Arctic Ocean sedimentation rates (for example Backman et al. 2004), however, meant that some negative inclination sequences could no longer be explained as having occurred in different polarity chrons. This problem also highlighted the importance of accurate age models, and showed how weak age models could yield incorrect sedimentation rates and distorted chronologies. Magnetic excursions lasting tens of thousands of years were also proposed to account for the observed negative inclinations (e. g. Løvlie et al. 1986), but these were later deemed incompatible with the duration of excursions thought to be less than 5 thousand years (Laj and Channel, 2007; Xuan and Channell, 2010). In their study of ACEX cores, O'Regan et al. (2008) cited postdepositional processes as a possible factor altering the chronological boundaries of preserved geomagnetic signals, and warned that relying on magnetic inclination data only, was problematic. Channel and Xuan (2009) explained the broad intervals of the negative inclinations in Arctic Ocean sediments as the result of partially self-reversed chemical remanent magnetisation.

Describing features of the magnetic field is essential in order to overcome some of these difficulties. This requires observations through time, as the field is not constant, but exhibits changes both in direction and intensity over time – referred to as secular variation. Observing secular variation, particularly on relatively short (few thousand years) timescales, can provide valuable information on fluid motions within the core and on the geomagnetic field behaviour, and could also allow the identification of patterns similar to those

observed over the last few centuries; but it demands well dated (and ideally continuous) records (Bourne, 2016). Naturally, marine sedimentary sequences can offer continuous palaeomagnetic records, however, records capable of preserving centennial – millennial scale changes are scarce from the Arctic region, primarily due to logistical difficulties, low sedimentation rates, and the paucity of datable material in Arctic sediments. The few records available suffer from the lack of accurate chronologies (St-Onge and Stoner, 2011). It is therefore essential to produce high-resolution Arctic palaeomagnetic records, which are supported by a robust chronology.

In recent years, a number of palaeomagnetic studies on Western Canadian- and Alaskan Arctic marine sedimentary sequences emerged, and focused on addressing chronostratigraphic issues in the area. Barletta et al. (2008) showed the correlation of palaeodirections from two Western Canadian Arctic cores (2004-804-803 and HLY0501-05JPC) with North American lacustrine and volcanic records. Lisé-Pronovost et al. (2009) examined two cores from the Chukchi Sea (HLY0501-06JPC and JLY0501-08JPC), providing further invaluable constraints on the regional Holocene chronostratigraphy (for core locations see Figure 2). Barletta et al. (2010) highlighted how spherical harmonic models of the geomagnetic field, such as CALS7k.2 could serve as an additional dating tool. A further palaeosecular variation (PSV) record (based on three sediment cores) from the Chukchi Sea was found to be consistent with the above studies by Lund et al. (2016), who also concluded that the virtual geomagnetic dispersion record of the studied cores is markedly different from those of lower latitudes (N 50° – 60°), which lie outside the surface expression of the tangent cylinder.

These studies indicate how palaeomagnetic investigations can be used as a powerful toolset to overcome the difficulties experienced when dating Arctic sedimentary sequences, and they also reveal the complexity of uncovering the geomagnetic signal at high latitudes. However, they rely on a relatively small number of radiocarbon dates, and thus lack strong chronologies necessary for providing a high-resolution, centennial-millennial scale palaeomagnetic record.

Therefore, the specific aims of the current study are to:

- Produce, a well-dated (14 radiocarbon dates), high-resolution, Holocene palaeomagnetic secular variation (PSV) record using a piston core (SWERUS-L2-2-PC1) retrieved from the northwestern Chukchi Sea.
- Compare the obtained PSV record with geomagnetic model predictions and other Low-Arctic (N 69° - 74°) PSV records in an attempt to improve the chronological constraints for geomagnetic variability in the Western Arctic.
- Provide insights into the nature of geomagnetic field behaviour in the Arctic.

2. Regional setting

The studied piston core, SWERUS-L2-2-PC1 (2PC1) was recovered from a site (N 72.51658°, W 175.319605°) located in the Herald Canyon (water depth 57 m), western Chukchi Sea (Figure 2) during leg 2 of the SWERUS-C3 2014 Expedition on icebreaker *Oden*.

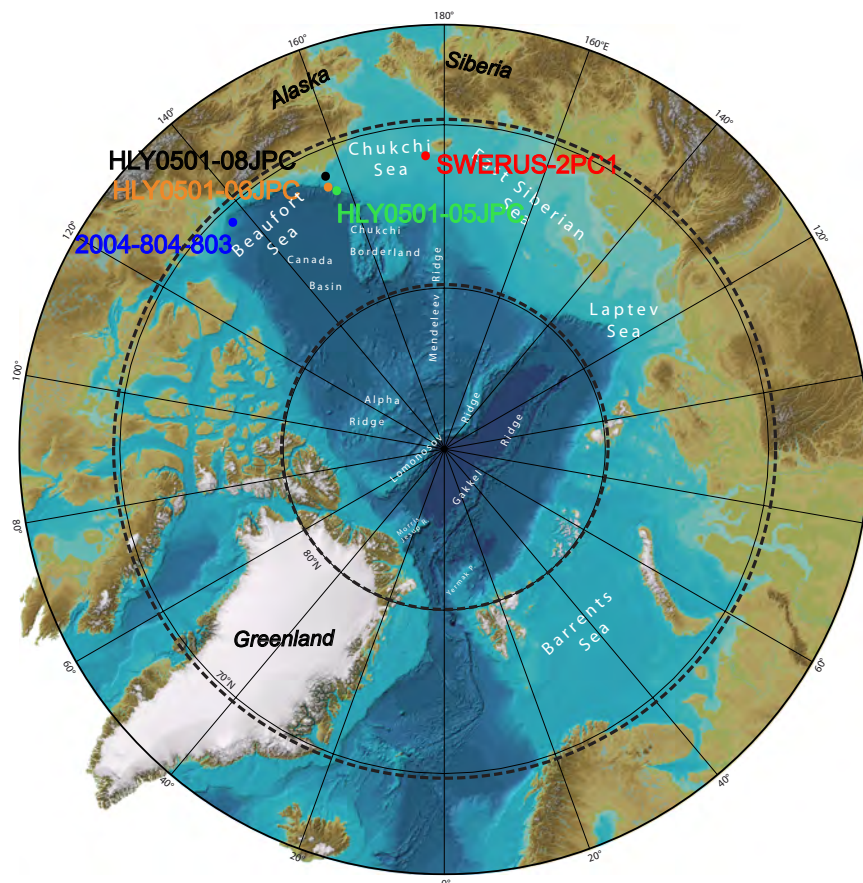


Figure 2: Location of the SWERUS-2PC1 core. Approximate locations of the cores referred to in the Introduction are also displayed. The black dashed lines at 69.5° and 80° N latitude mark approximate locations where a hypothetical tangent cylinder would cut the core-mantle boundary and the surface of the Earth respectively. The map is based on the International Bathymetric Chart of the Arctic Ocean (Jakobsson et al. 2012).

The Chukchi Sea is a relatively shallow (~50 m) shelf sea (Weitgartner et al., 2005), which lies north of the Bering Strait. Pacific water entering the Bering Strait splits into a number of distinctive water masses (Weitgartner et al., 2005; Spall, 2007; Pickart et al., 2009), the most westerly of which flows through Herald Canyon (Figure 3). There appears to be a significant difference in the eastern and western sides of the Canyon, both in terms of water masses and flow regime (Pickart et al. 2009), with a strong (reduced in winter) northward flow (direct from the Bering Strait) observed on the eastern side within which the 2PC1 core site is located. Pickart et al. (2009) argued that the western side of the Canyon is fed by a winter water reservoir located just southeast of

Wrangel Island, and the resulting flow switches sides as it progresses northward, and while doing so, its turbidity greatly increases. This increased turbidity could partly explain the thicker sediment layer on the eastern side of the Canyon observed by Jakobsson et al. (2017).

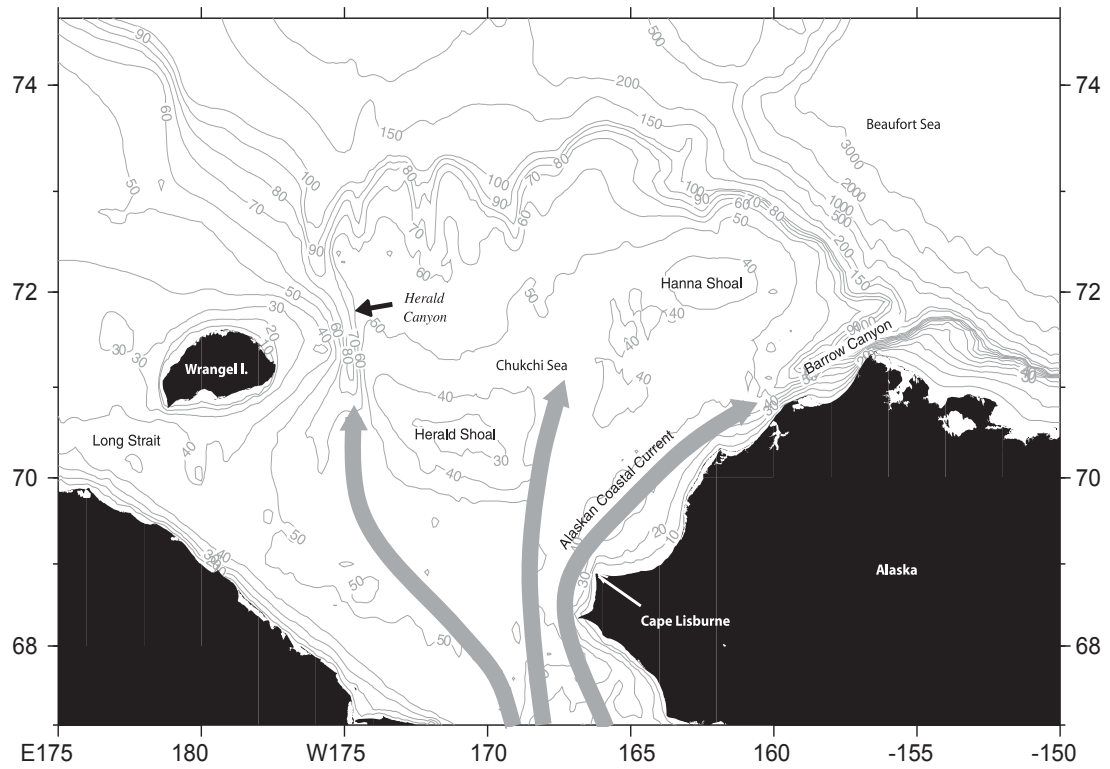


Figure 3: Schematic representation of branches of the Bering Strait inflow water (Pickart et al. 2009).

3. Age model and Lithology

The age – depth model (Figure 4) used for the current study was established by Pearce et al. (2017) who utilised radiocarbon (^{14}C) dating of molluscs (14 dates in total), and the identification of an ash layer associated with the Aniakchak eruption of 3600 years BP. The authors calculated a radiocarbon marine reservoir age of 477 ± 60 years, and argued that its resemblance to present day values could suggest a constant marine reservoir age for the Chukchi Sea during the second half of the Holocene. The age estimate for the bottom of the core was 4250 ± 115 cal years BP.

An average sedimentation rate of 200 cm / ka was determined. This is a very high value for the Holocene Arctic in general, but not unusual for shallow shelf areas and continental slopes (Backman et al. 2004; Darby et al. 2009; Wegner et al. 2015). The sedimentation rate appears relatively constant for 2000 – 4200 years BP interval, reaching a minimum between 1000 – 2000 years BP, before undergoing a sharp increase from ~ 1000 years BP to reach the current level of about 3 m/ka (Figure 4).

The lithology of the core is relatively homogeneous, dominated by olive grey – grey clay, and silty clays. There are no abrupt changes in the various physical properties, including the multi-sensor track derived bulk density, total organic carbon content, and porosity (Figure 5). The SWERUS-C3 Expedition team (2014) also observed occasional black horizons and mottling (possibly iron-monosulphide), shell fragments, and a distinct cream /orange coloured nodule (2 x 2 cm) at about 5.87 metres below seafloor (mbsf), clearly visible on the core digital image (Figure 5; Appendix I). These could indicate postdepositional processes, which can alter the magnetic mineralogy.

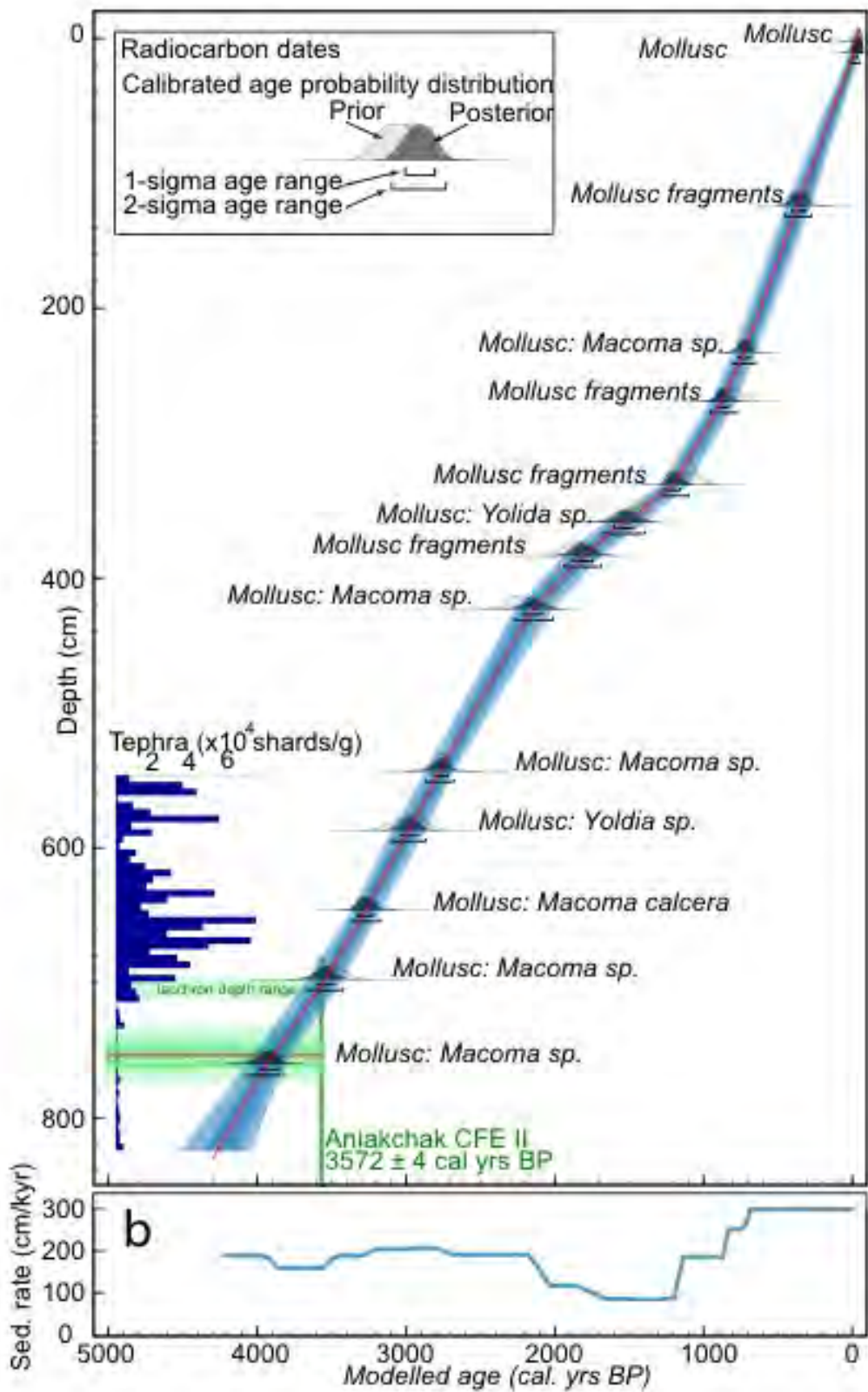


Figure 4: Age - depth model and sedimentation rate of core 2PC1. Modified after Pearce et al. (2017).

Some distinctive shifts can be observed in the shipboard whole core magnetic susceptibility record (Figure 5). Major peaks are visible in the 3–4 mbsf, and 6 – 7 mbsf depth range. Between 4 – 6 mbsf, the susceptibility values are lower than the rest of the core. The Ca / Fe ratio, which can indicate marine and terrigenous inputs appears to resemble the susceptibility trend (Rothwell and Croudace, 2015).

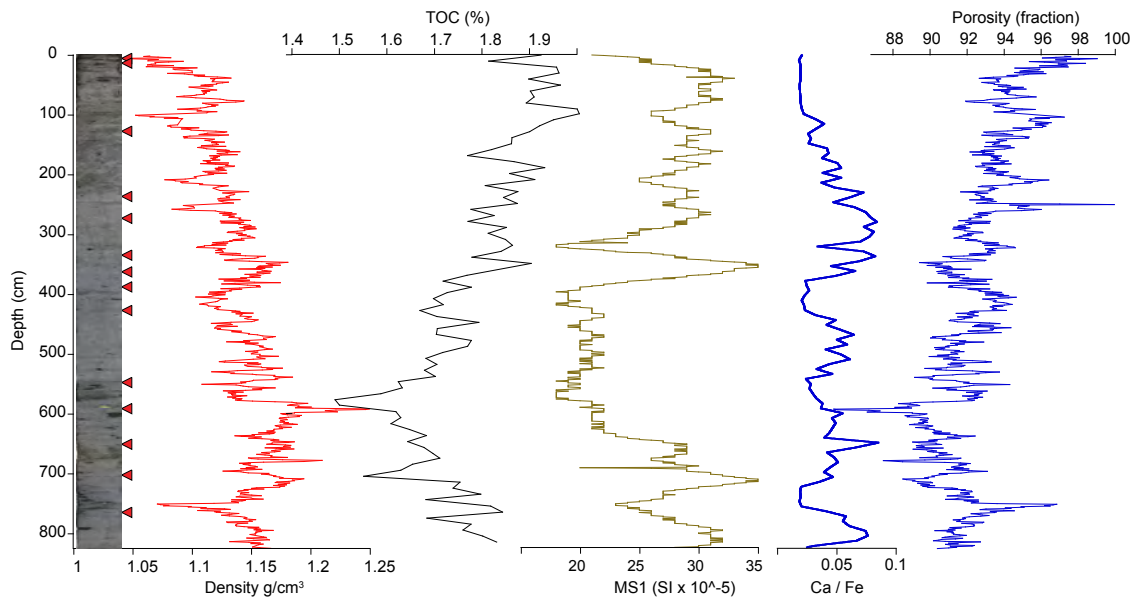


Figure 5: Core digital image (Cronin et al. 2017), bulk density, TOC, magnetic susceptibility, Ca/Fe ratio and porosity profile of core 2PC1

No significant oscillations can be observed in the high resolution XRF analysis

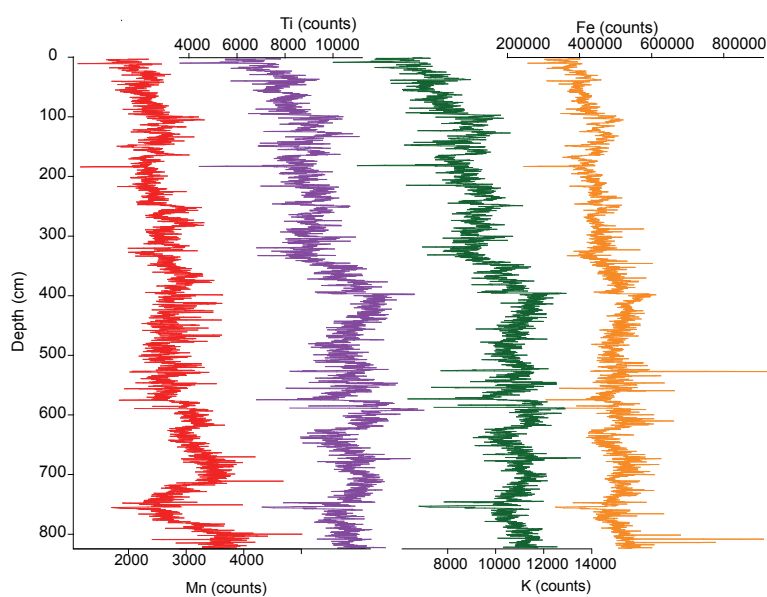


Figure 6: XRF elemental analysis of core 2PC1: Mn, Ti, K and Fe concentration variability with depth

of manganese (Mn), titanium (Ti), potassium (K) and iron (Fe) concentrations (Figure 6), apart from a very sharp drop in all values observed at 5.87 mbsf. These anomalously low values only characterise a ~2 cm interval corresponding to the orange nodule, so they are not displayed on the

figure. Calcium concentrations at this depth are exceedingly high, indicating calcium as a compositional element for the nodule. The iron profile appears to correlate with the titanium and potassium records. Titanium often linearly varies with coarse-grained terrigenous fraction, thus the increase in concentration below ~3.5 mbsf depth could signal a larger terrigenous continental input (Rothwell and Croudace, 2015). There are no notable intervals where variations in manganese and iron, both redox sensitive elements, differ markedly from more conservative elements like titanium.

4. Materials and Methods

a. Core description and sampling procedure

The SWERUS-2PC1 core was retrieved at a water depth of 57 metres. During coring, a Star-Oddi DST magnetic orientation sensor was attached to the core barrel, which recorded temperature, pressure (depth), compass heading of the sensor and core tilt (O'Regan et al. 2016). The sensor recorded an azimuth of 175°, and a core tilt of 18.5°. The relatively high core tilt was presumably caused by the shallow water and considerable vessel drift.

The core measured 8.28 metres with 92% recovery. It was split lengthwise into six sections (Figure 7), and stored at 4°C shipboard, and later at the Department of Geological Sciences, Stockholm University.

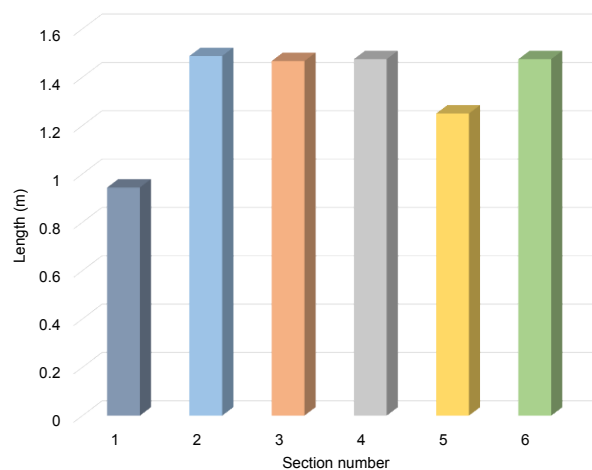


Figure 7: Section lengths of core 2PC1

Palaeomagnetic discrete subsamples were collected from the archive halves of the core at 2.5 cm intervals. Standard nonmagnetic plastic sampling boxes of 2.2 cm x 2.2 cm x 2.3 cm dimensions (with an internal volume of approximately 7 cm³) were used. Specimen IDs started at 001, and increased downcore in steps of 1. The sampling frequency yielded 320 discrete specimens. 2 sample cubes (specimen ID 226 and 227) were not filled due to the presence of the cream / orange coloured nodule observed at ~ 5.87 mbsf.

b. Palaeomagnetic measurements

i. Magnetic susceptibility

Magnetic susceptibility (κ) was measured using a Kappabridge MFK1-FA modular system at the Department of Geological Sciences, Stockholm University. Induced field was 425 A /m. The magnetic susceptibility data have then been analysed using AGICO's Anisoft4.2 software (Chadima and Jelínek, 2008) to establish downcore variation and anisotropy of magnetic susceptibility.

In order to calculate mass normalised susceptibility values, each specimen was weighed using a Sartorius M-pact Series Ax623 electronic analytical and precision balance (with repeatability ± 0.002 and linearity ± 0.004). For specimen weight data see Appendix II.

ii. Natural remanent magnetisation (NRM)

Natural remanent magnetisation of the specimens was measured and then progressively demagnetised using a 2G Enterprises 2G760 superconducting rock magnetometer at Lund University Palaeomagnetic Laboratory. Initially, pilot subsamples were used, selected at every 50 cm, utilising peak alternating fields (AF) of 5, 10, 15, 20, 25, 30, 35, 40, 45, 50, 60, 70, 80 and 100 mT. Assessment of the pilot subsample data revealed that the ChRM magnetisation could be identified between AF strengths of 20 – 80 mT, so stepwise demagnetisation utilised peak AF of 5, 10, 15, 20, 25, 30, 40, 50, 60, and 80 mT. Standard principal component analysis (PCA) of Kirschvink (1980) has been applied to the NRM measurements for the 20 – 80 mT peak field range in order to isolate inclination and declination of the characteristic remanent magnetisation (ChRM) of the specimens. Median destructive field (MDF) of the NRM and maximum angular deviation (MAD) values were also determined

during the PCA analysis (Appendix III). The PCA analysis was performed with the DAIE software of Sagnotti (2013).

The MDF is the field required to reduce the magnetisation to half of its initial value and can be used as a proxy for magnetic grain size and magnetic mineralogy. MAD values can serve as a precision tool for the measurements, as MAD values greater than 5° often indicate a complicated magnetisation of the sediments and hence should be treated with care (Stoner and St-Onge, 2007). As an 18.5° core tilt was indicated by the Star-Oddi DST sensor, a correction of this magnitude was applied to the measurements.

iii. Anhyseretic remanent magnetisation (ARM)

Following stepwise demagnetisation of the NRM, anhyseretic remanent magnetisation was imparted using the same 2G Enterprises 2G760 superconducting rock magnetometer. A peak alternating field of 100 mT with a 0.05 mT direct current biasing field was used on the Z axis of specimens with an even sample ID number (50% of all specimens). The ARM was then measured and stepwise demagnetised at peak fields of 10, 20, 30, 40, 60, and 80 mT. Anhyseretic susceptibility, κ_{ARM} was also determined by normalising the ARM with the direct current biasing field. In order to estimate changes in magnetic grain size, the κ_{ARM} was divided by the magnetic susceptibility ($\kappa_{\text{ARM}} / \kappa$).

iv. Isothermal remanent magnetisation (IRM)

Isothermal remanent magnetisation was imparted using a Redcliff 700-BSM pulse magnetiser to the Z axis of the specimens with a direct current pulse field of ~1 T (1.02 T), followed by demagnetisation with the 2G720 magnetometer at 10, 20, 30, 40, 60 and 80 mT peak fields. As this field was the highest available field in the current study, in the following, IRM is referred to as saturation isothermal remanent magnetisation (SIRM). Due to time and

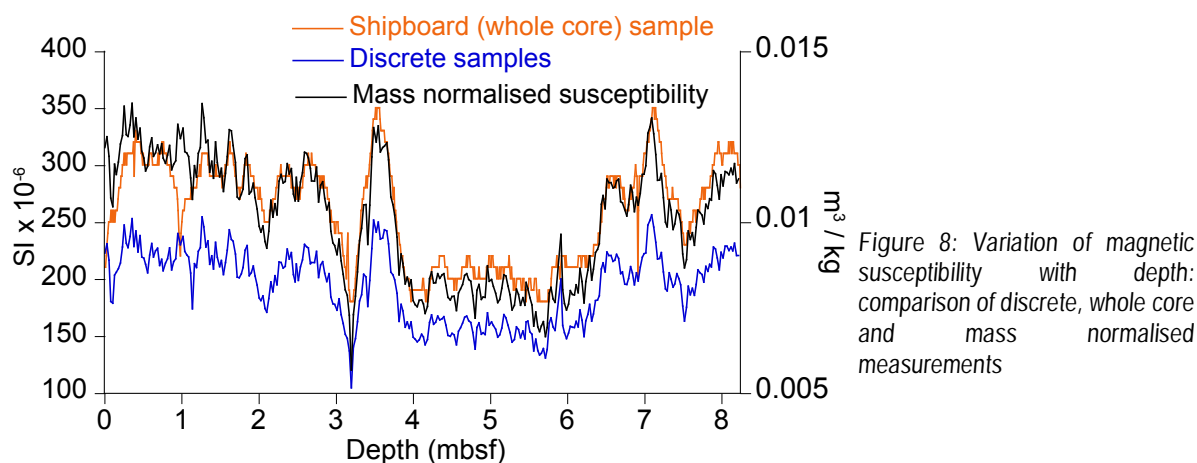
cost constraints, only specimens with even sample IDs up to sample ID 196 were measured (~30% of all specimens).

ARM and IRM are laboratory induced magnetisations, which primarily depend on changes in the concentrations of magnetic materials in the sediment core. As such, not only are they useful indicators for changes in the magnetic mineralogy, but can also be utilised in relative palaeointensity (RPI) calculations.

5. Results

a. Magnetic susceptibility and anisotropy of magnetic susceptibility

Mean magnetic susceptibility (volume) of all specimens is 193.5×10^{-6} SI, ranging from 104.4 to 256.2×10^{-6} SI. Volume susceptibility measured on the discrete sediment samples was compared with the shipboard whole core measurements, and following mass normalisation, with the mass normalised susceptibility (Figure 8). Variation of magnetic susceptibility with depth shows identical pattern in the three sets of measurements.



Anisotropy of magnetic susceptibility (AMS) can be generated by the statistical orientation of the magnetic grains, and is best characterised by the orientation and strength of three orthogonal axes (commonly referred to as principal axes) of the susceptibility ellipsoid: K_{\max} , K_{\min} , K_{int} . Orientations of the principal axes, K_{\max} (blue squares), K_{int} (green triangles) and K_{\min} (purple circles) were plotted on an equal-area projection for all specimens (Figure 9), and then for individual core sections (Figure 10). The sediment fabric is characterised by an oblate AMS ellipsoid typical of sedimentary sequences, with K_{\min} directions perpendicular to the bedding plane.

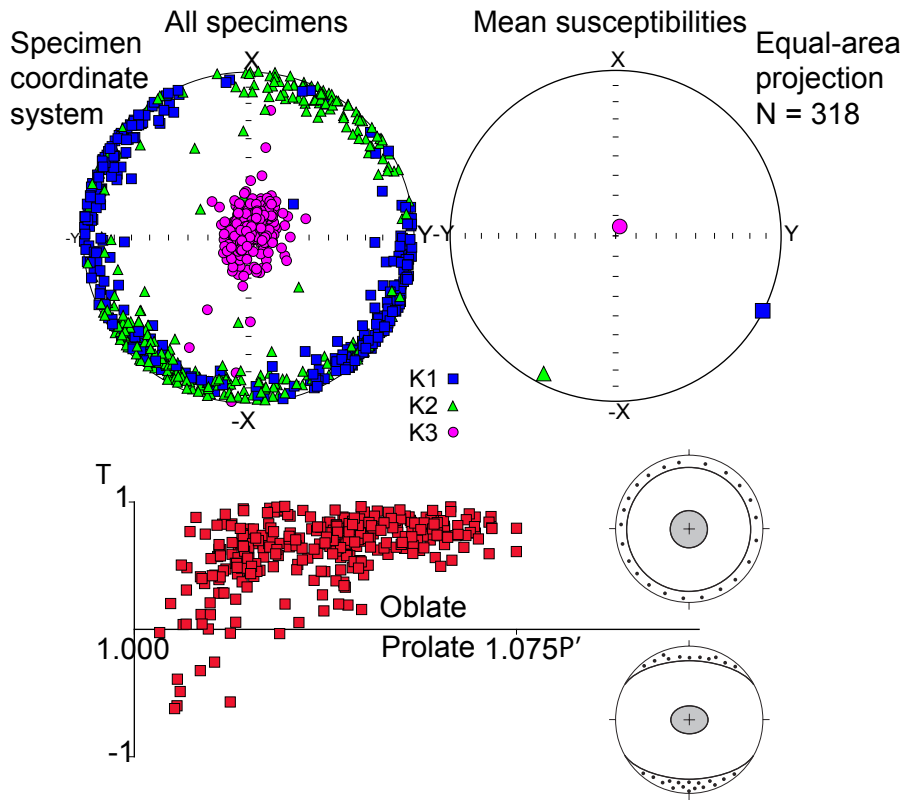


Figure 9: Anisotropy of magnetic susceptibility for 318 specimens from core 2PC1. The orientations and mean directions of the principal axes, and corrected anisotropy degree against the shape parameter are shown. Representative images of the oblate and prolate ellipsoids (bottom right) display the foliation poles (shaded) and the lination (dotted area) – image taken from Archanjo et al. (2006).

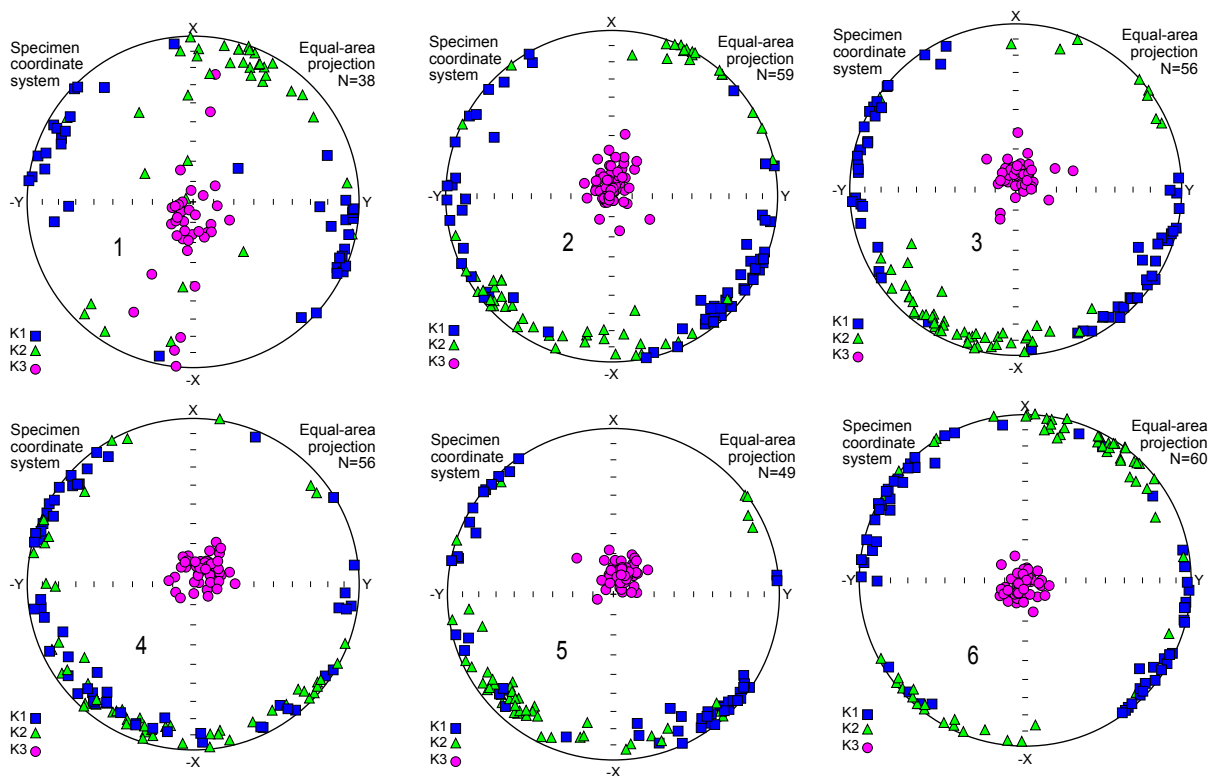


Figure 10: Anisotropy of magnetic susceptibility for core sections 1 - 6, displaying the distribution of the principles axes

b. Natural remanent magnetisation and palaeomagnetic directional data

Stepwise demagnetisation curves and vector end point diagrams (Zijderveld, 1967) were prepared for all specimens to observe direction and intensity changes during demagnetisation. Such demagnetisation curves and Zijderveld plots for three representative specimens (ID 018, 152, 208) are displayed (Figure 11). The demagnetisation curves illustrate the progressive decay of

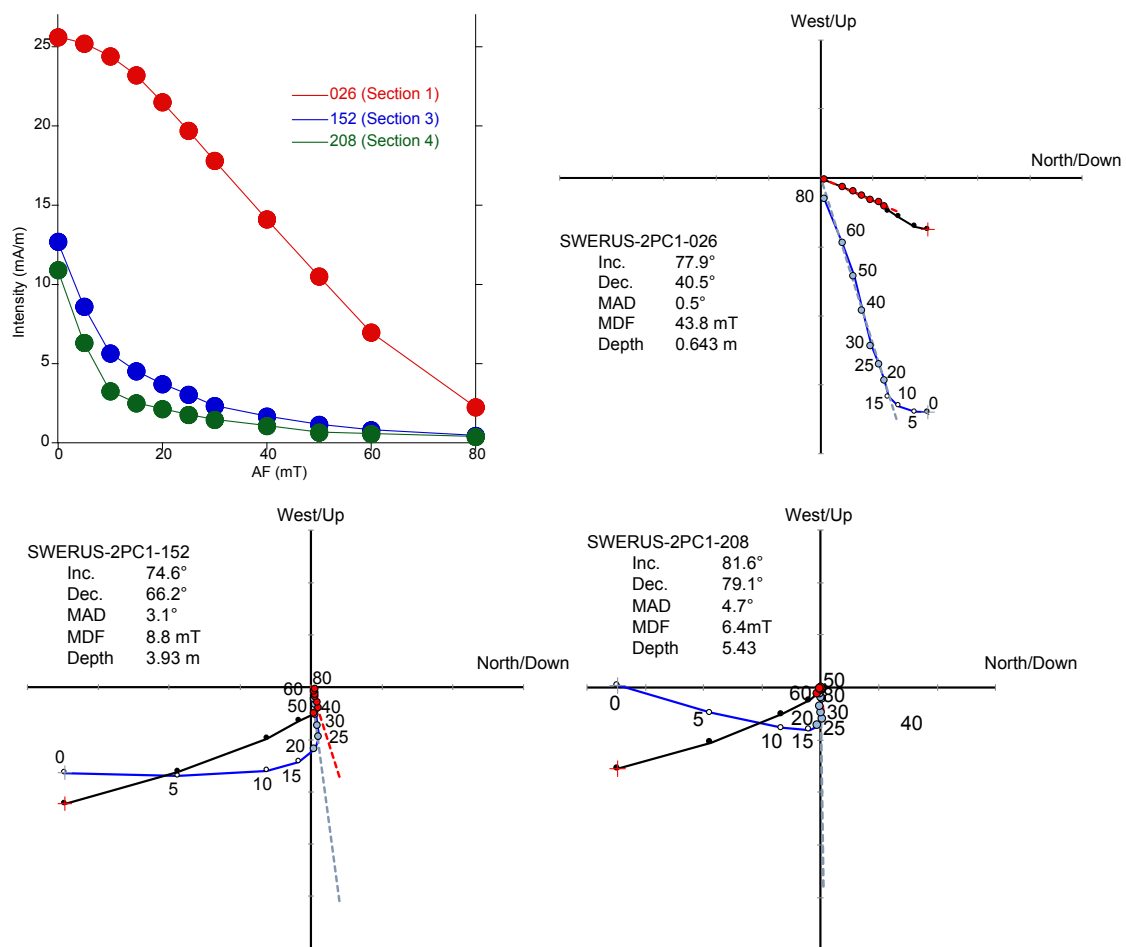


Figure 11: Stepwise demagnetisation curves for representative samples, and the corresponding Zijderveld diagrams. Zijderveld plots modified after the DAIE software of Sagnotti (2013).

the magnetisation with increasing demagnetisation level. Distinct changes in slope direction are indicative of different stability components of the NRM, with low-stability components easily demagnetised. The direction of the NRM appears constant between levels of 20 and 80 mT, suggesting a strong ChRM between these demagnetisation levels. This is also apparent in the Zijderveld plots, which display horizontal (red), and vertical (blue) components of the NRM

vectors. Points between 0 and 20 mT seem to be collinear, and similarly, points between 20 and 80 mT also appear collinear. However, the direction of the trajectory lines is different: only the second set (20–80 mT) points towards the origin. This is a clear indication of two separate components of the NRM: one is removed between 0 and 20 mT, the other one is removed between 20 and 80 mT.

Downcore variations of the NRM intensity, the MDF, the ChRM inclination and declination are presented with the corresponding maximum angular deviation (MAD) values calculated for the 20–80 mT peak alternating field range (Figure 12 and Table 1).

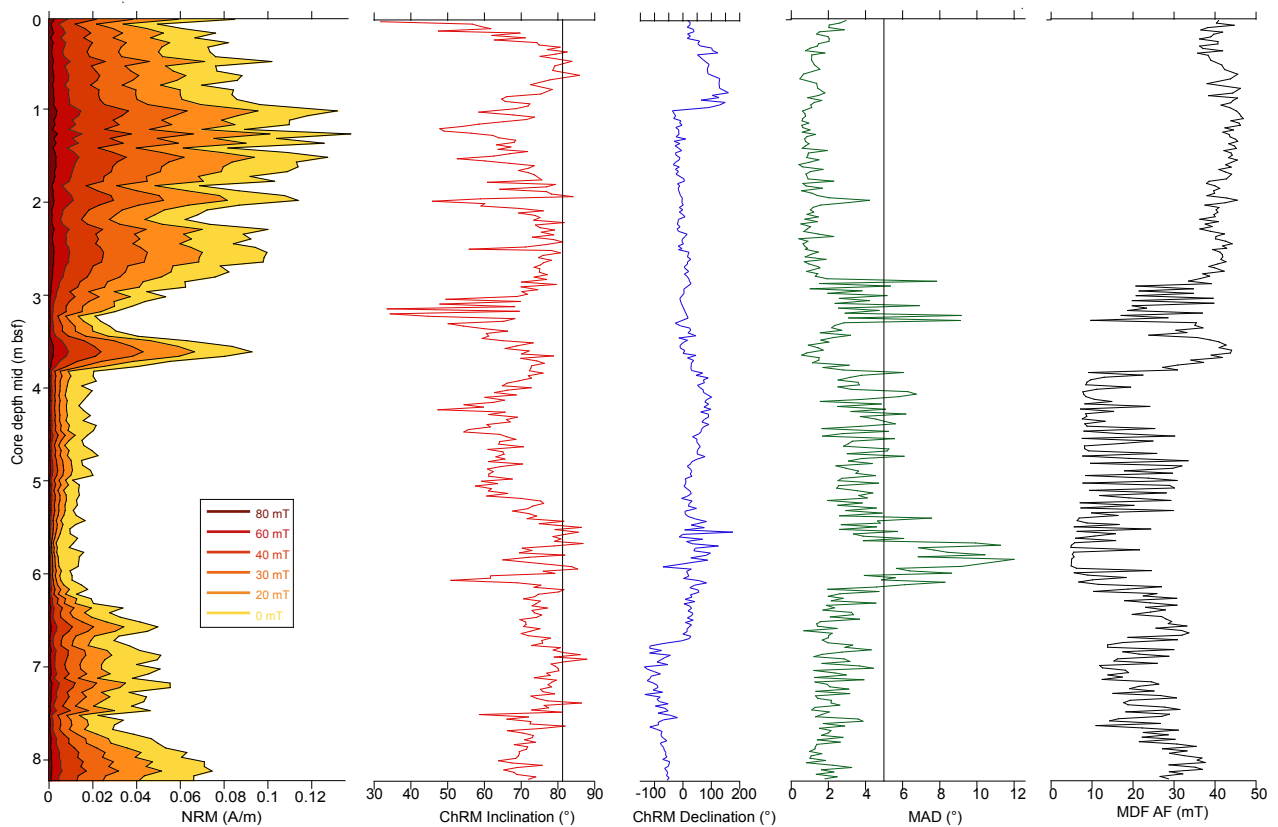


Figure 12: Downcore variation of the ChRM NRM, inclination, declination with MAD values calculated for the 20–80 mT peak alternating field range and median destructive field (MDF) of the NRM. Vertical grey lines indicate the GAD expected value of 81°, and the MAD value of 5° for the inclination and MAD profiles respectively.

	NRM intensity (A/m)	Inclination (°)	Declination (°)	MAD (°)	MDF (mT)
Arithmetic mean	1.73 x 10 ⁻²	70.1	11.6	2.7	28.1
Median	1.68 x 10 ⁻²	71.8	15.0	2.1	29.8
Standard deviation	8.6 x 10 ⁻³	8.9	60.6	2.1	12.8
Minimum value	2.77 x 10 ⁻³	31.8	-134.2	0.4	4.9
Maximum value	3.73 x 10 ⁻²	87.9	171.8	12.0	46.9

Table 1: Key descriptive statistical parameters for NRM intensity, ChRM inclination, declination, MAD and MDF.

The NRM intensity signal varies between 2.77 and 37.3 mA/m for the core, with the maximum value found at 2.01 metres below seafloor (mbsf). The intensity sharply drops to about half of its mean value at about 3 mbsf, then recovers between 3–4 mbsf before dropping once again and achieving a mean intensity of 7.6 mA/m for the 4 – 6 mbsf depth range, which is less than half of the mean (17.3 mA/m) for the whole core.

The ChRM inclinations vary around 70°, which is below the expected value of 81°, as predicted by the geocentric axial dipole (GAD) model for the core location. According to the GAD model, inclination varies as a function of latitude: $\tan I = 2 \tan \lambda$ (where I = inclination, and λ = latitude).

In order to provide a continuous declination record, scale adjustment was applied to account for circular values (0° and 360°). Abrupt linear changes can be observed in the ChRM declination record at the Section 1 and 2, and the Section 5 and 6 boundaries, indicating that possible unwanted section rotation occurred. The declination values appear elevated between 4–5 mbsf when compared to the rest of the core, and also show an oscillating pattern at the 5.5 – 6 mbsf depth range.

Arithmetic mean of the MAD values is 2.7° with a maximum value of 12°, and 85.5% of all MAD values falling below 5°, indicating very well defined NRM component directions. There is a marked increase in MAD values in the 5.6 – 6 mbsf depth range, coupled with an increased mean value of 7.5°.

The median destructive field (MDF – the peak AF field required to reduce the NRM to half of its initial value) of the NRM averages at 28.1 mT, typical for magnetite as the main carrier of the ChRM. A marked fluctuating pattern and reduced values can be observed between approximately 4 and 6 mbsf. Reduced MDF values could indicate grain size coarsening.

c. Magnetic grain size and concentration

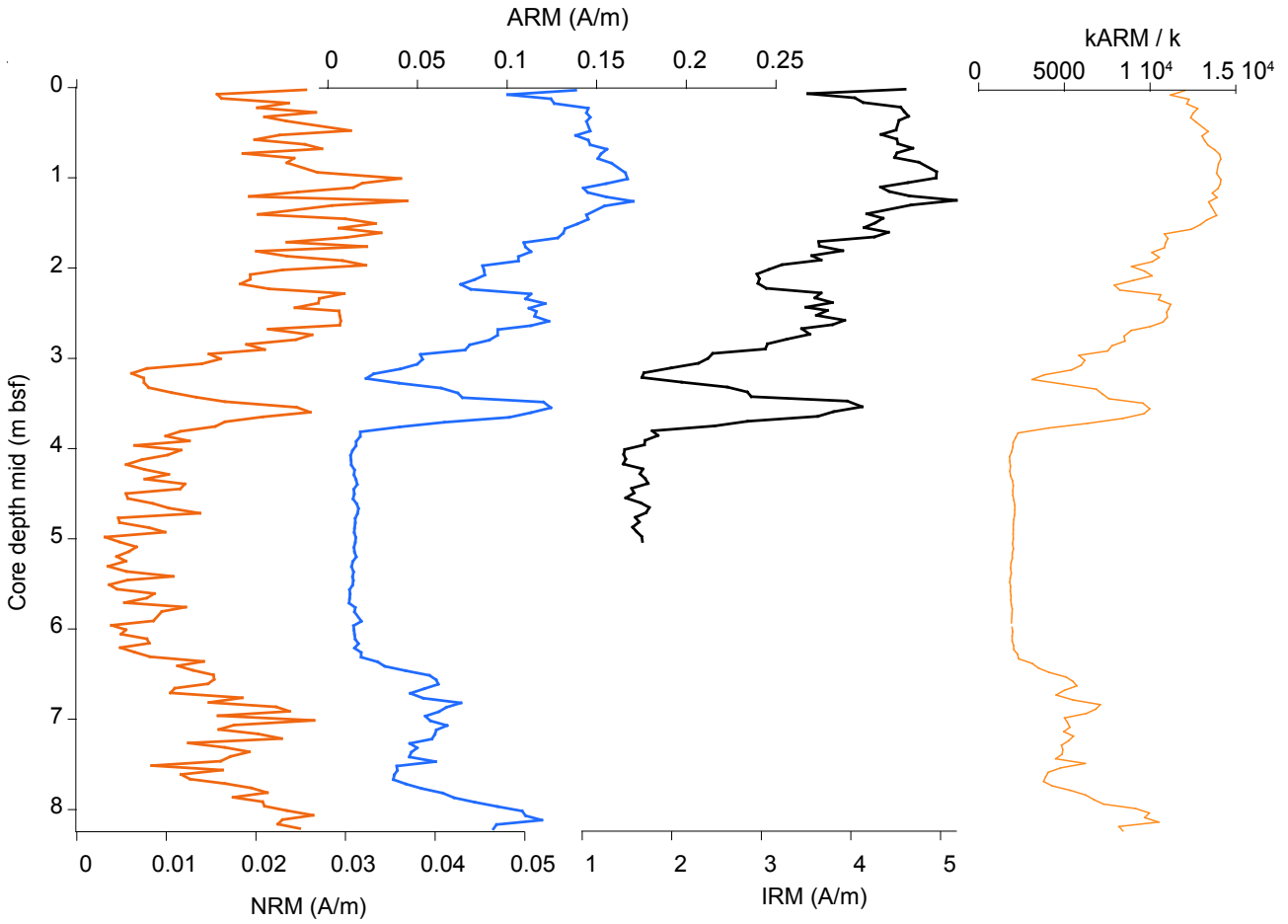


Figure 13: NRM, ARM and SIRM intensities. Note, the SIRM signal is only available up to 5 mbsf.

Downcore variations in the ARM and SIRM intensities display similar behaviour to the NRM intensity signal, as revealed by a comparison (Figure 13). Significant reduction in the ferrimagnetic concentration, particularly in the 4 – 6 mbsf depth range can be observed. Not only the concentration of ferrimagnetic grains changes in this depth range, but the magnetic grain size also shows a significant increase, as indicated by the grain size sensitive anhysteretic susceptibility (κ_{ARM}) normalised by magnetic susceptibility (κ). This ratio (κ_{ARM}/κ) inversely varies with magnetic grain size, assuming magnetite dominates the magnetic mineralogy (Lisé-Pronovost, 2009). This suggests that a coarsening of the magnetic grain size occurs in the 4 – 6 mbsf depth range.

This is further confirmed by examining the relationship between κ_{ARM} and magnetic susceptibility, which is strongly grain size dependent (Maher and Hounslow, 1999). The bivariate plot of κ_{ARM} and κ (Figure 14) allows the identification of different grain size ‘clusters’ (King et al, 1982), and indicates a clear variation of magnetic grain size with depth, also shown by the changes in the slopes of the regression lines. The drop in the slope of the line characterising the top 3 metres of the core most likely points towards a downcore decrease in the amount of fine grained magnetite, with the lowest amounts between 4–6 mbsf.

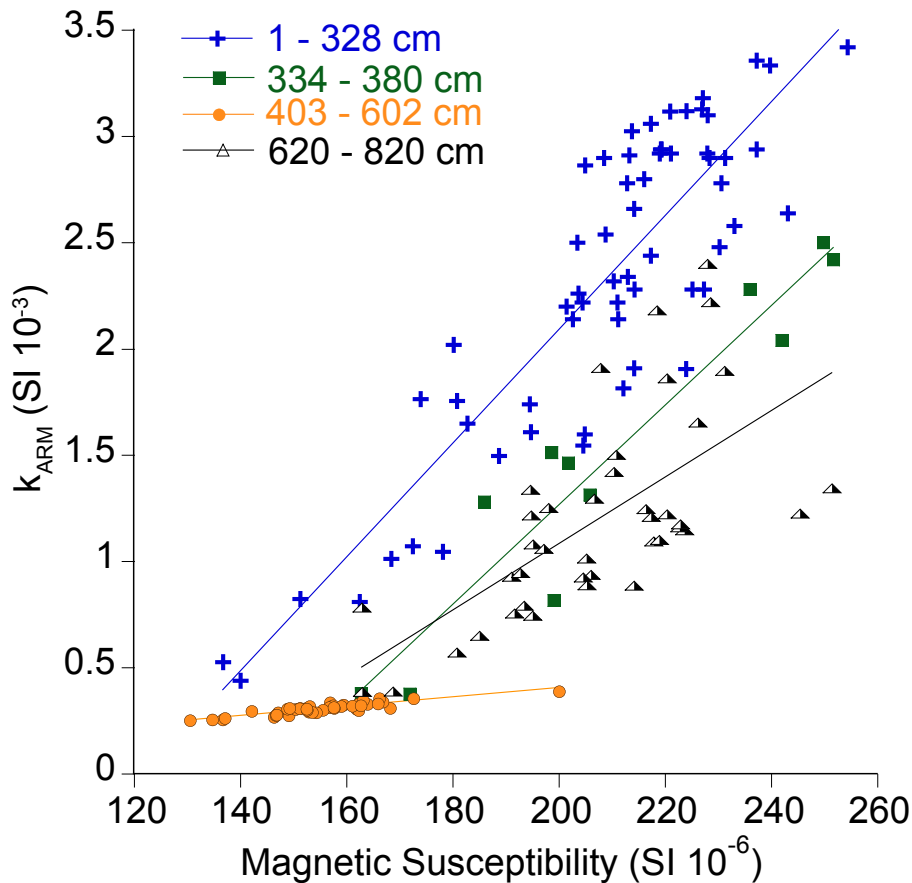


Figure 14: Changes in grain size with depth as indicated by the relationship between the k_{ARM} and magnetic susceptibility.

d. Relative palaeointensity determination

Although marine sedimentary sequences can provide continuous palaeointensity records, variations in factors which control the magnetisation of sediments, such as the magnetic content of the sediments, can dominate and thus distort the intensity signal (Tauxe, 1993). In order to reduce this effect, and to obtain a palaeointensity record, overprints of factors other than the ambient field (for example changes in the concentration and grain size of ferrimagnetic materials) have to be removed. This is achieved by normalising the NRM with a magnetic grain size- or concentration-dependent normaliser, such as magnetic susceptibility, ARM, anhysteretic susceptibility, $\kappa_{\text{ARM}} / \kappa$, or SIRM (Evans and Heller, 2003). No general consensus exists over the preferred

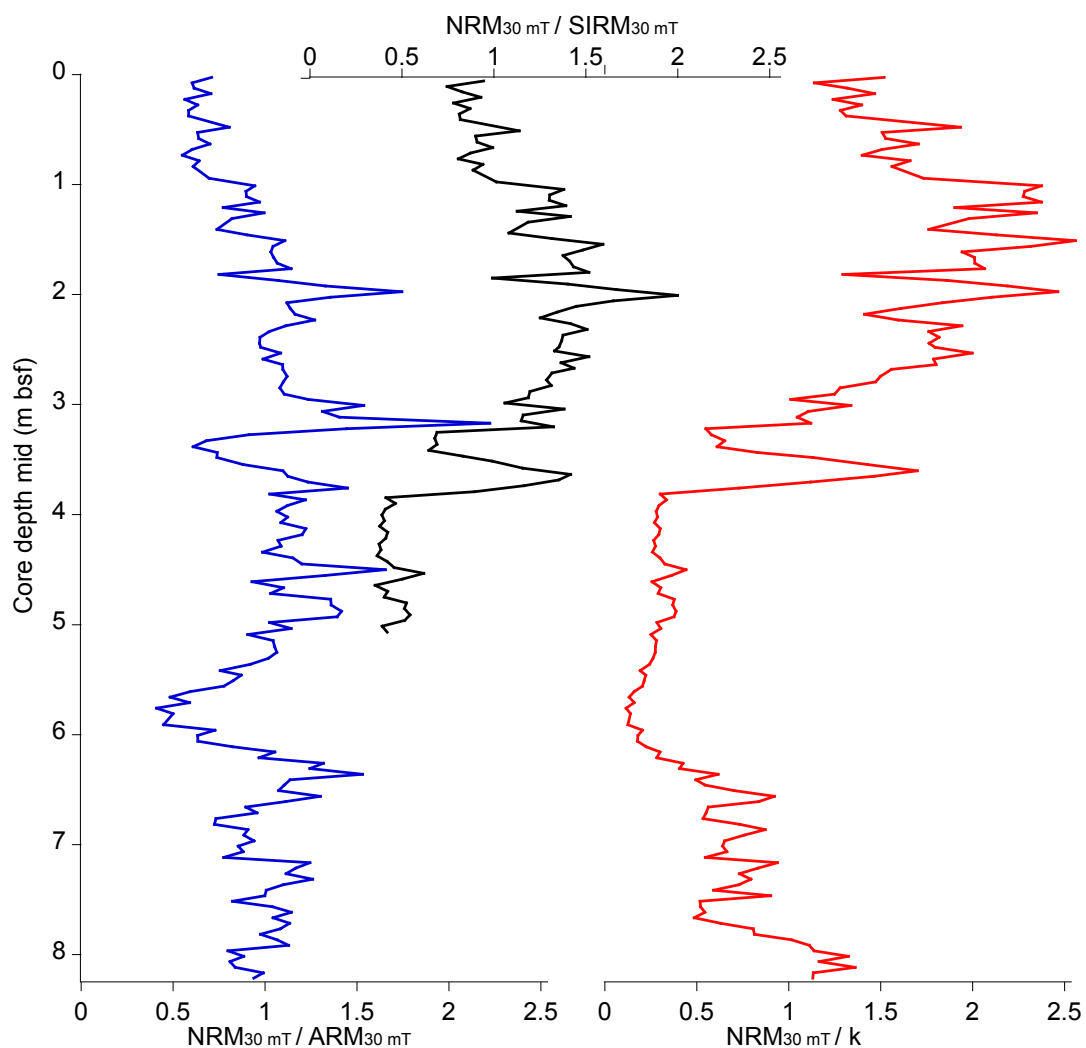


Figure 15: Relative palaeointensity record of core 2PC1

normaliser (Valet, 2003), but the normaliser should be coherent with the NRM signal, and it should have no correlation with the normalised NRM. RPI estimates which show coherence with bulk rock magnetic parameters also require caution (Tauxe, 1993).

The NRM signal at the 30 mT demagnetisation step has been normalised with the ARM_{30mT} , $SIRM_{30mT}$, and the magnetic susceptibility values in order to identify a preferred NRM normaliser. All three normalised records were divided by their arithmetic mean to allow inter-comparison (Figure 15). The $SIRM_{30mT}$ and magnetic susceptibility normalised RPI records follow a similar pattern, and display a strong resemblance with the NRM record ($r = 0.87$ and $r = 0.98$ respectively), thus the ARM was chosen as the preferred normaliser.

6. Discussion

a. Anisotropy of magnetic susceptibility

In marine sedimentary fabrics, orientation of the principle axes follows a characteristic pattern: K_{\min} is usually vertical, while K_{\max} and K_{int} are spread in the horizontal plane (Tauxe, 2007). In case of core tilting, the difference between the stereonet pole and the mean direction of the K_{\min} axes can be indicative of the tilt angle (Chen et al. 1995). According to the Star-Oddi DST measurements, tilting of the 2PC1 core during coring occurred, with a tilt angle of 18.5° . This implies that off-pole mean direction of the K_{\min} axis can be anticipated (Figure 16).

However, no such tilt can be seen in the equal area projection diagram of the mean directions of the principle axes (Figure 9), indicating that the fabric might have been disturbed during coring. This is further supported by the AMS profile of section 1 (Figure 10), which shows a slightly streaked K_{\min} distribution. No similar

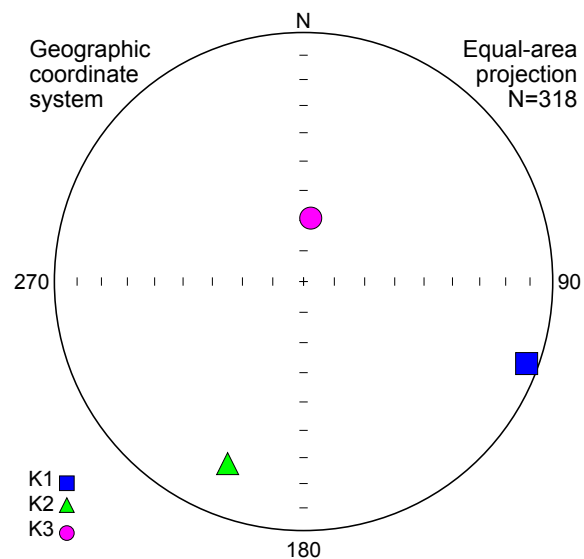


Figure 16: Expected mean orientations of the principal axes in case of an 18.5° core tilt.

distribution of the K_{\min} axes can be observed in the profiles of the other sections. The K_{\min} axes become progressively more clustered around the stereoplot centre downcore, and exhibit a slightly off-vertical distribution, characteristic of moderate current environments (Tauxe, 2007).

b. Comparison with geomagnetic field model outputs

Utilising the age–depth model of Pearce et al. (2017), the ChRM inclination and declination records, and the calculated relative palaeointensity signal of the core were compared with a number of computed geomagnetic field model outputs (A_FM; pfm9k.1a; CALS3K.4e; CALS10K.1b) to allow for the detection of common palaeomagnetic features during the last 4500 years BP (Figures 17 A, B, C).

A_FM (Licht et al., 2013) is an archaeomagnetic model. pfm9k.1a of Nilsson et al. (2014) is based on sediment data and was constructed after finding the best age–depth adjustments for each sediment record in order to reduce smoothing associated with inconsistent timescales. CALS3K.4e (Korte and Constable, 2011) is a high–resolution global geomagnetic field reconstruction model. Its time–varying spherical harmonic version, CALS10K.1b (Korte et al. 2011), spans the last ten thousand years, with a special focus on reflecting the large–scale field at the core–mantle boundary.

Comparison with these model outputs provides additional support for the reliability of the PSV record. For example, a number of similar inclination features can be readily identified in the profile of 2PC1 and the model outputs, in particular, between the 1000–2800 yrs BP time interval, during which period the character of inclination change is very similar. An inclination maximum for this period can be observed in the 2PC1 profile at around 1700 yrs BP, preceded and followed by a decline in values. This inclination spike is consistent with the field model predictions (especially with pfm9k.1a), but is somewhat reduced in duration: starting at about the same time (1200 yrs BP), but finishing approximately 100–200 years prior to the model outputs.

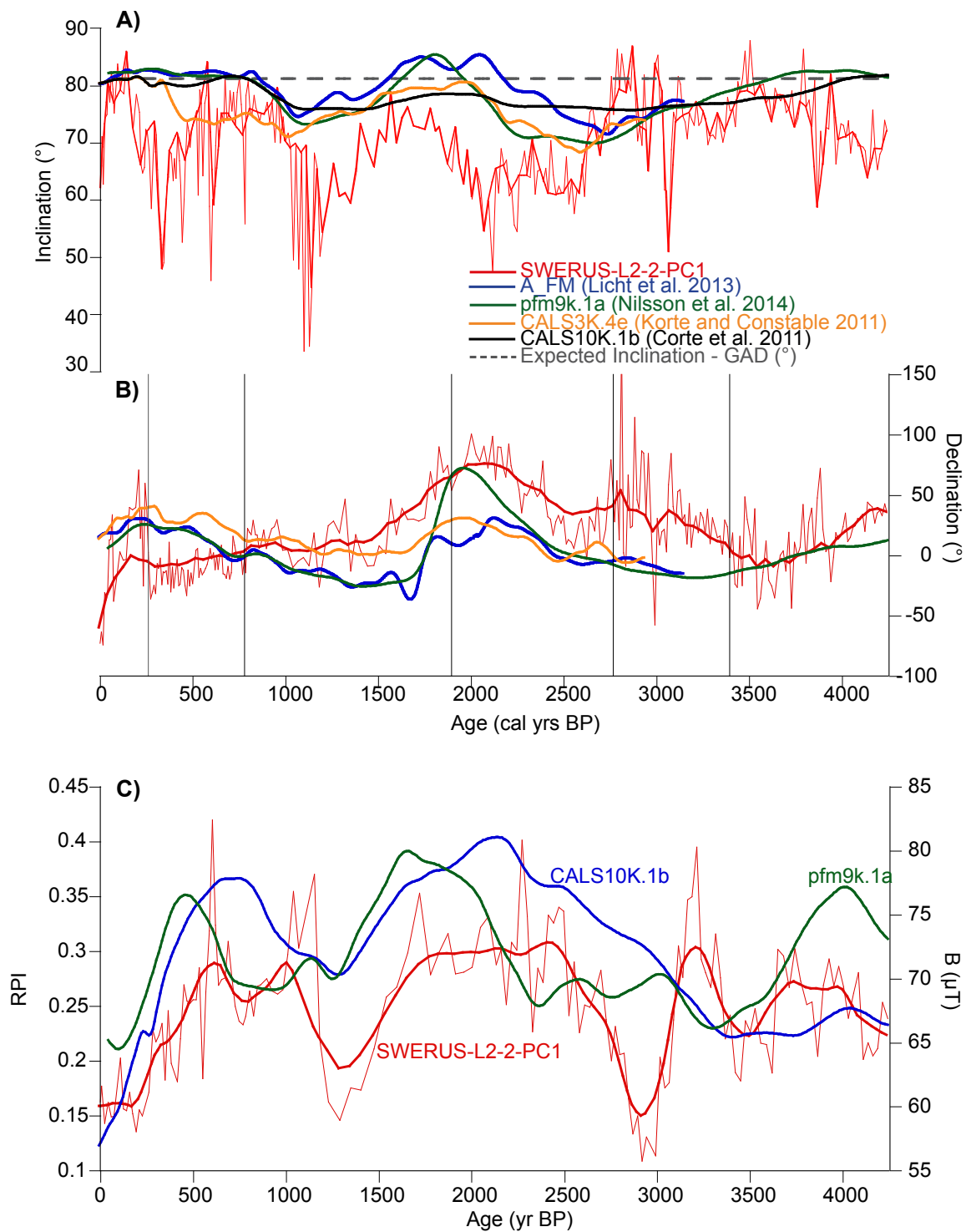


Figure 17: Comparison of the ChRM A) inclination B) declination record of core 2PC1 and expected values for the core location as predicted by the following models: A_FM (Licht et al. 2013), pfm9k.1a (Nilsson et al. 2014), CALS3K.4e (Korte and Constable, 2011), CALS10K.1b (Korte et al. 2011). The dashed line indicates the expected inclination for the site location according to a GAD ($\tan I = 2 \tan \lambda$). Vertical lines mark the core sections. Figure 13 C) displays the relative palaeointensity record for 2PC1, the CALS10K.1b (Korte et al. 2011) and pfm9k.1a (Nilsson et al. 2014) model intensity outputs for 2PC1 core location. The CALS10K.1b model output was generated using the GEOMAGIA50.v3 database (Brown et al. 2015). The smoothing fits were based on locally weighted (1%) least squares error method for the inclination profile, and geometric weights for the declination and RPI profiles (Kaleidagraph software).

Furthermore, during this same period (1000 – 2800 yrs BP, corresponding to 3 – 6 mbsf) the inclination values are shallower than the model signals, with values $\sim 10^\circ$ lower than expected by the GAD model (81°) for the core location, although, the GAD value is still within two standard deviations of the arithmetic mean (mean = 70.1° , sd = 8.9°). Inclination shallowing of sediments itself is a well-documented issue in marine sedimentary sequences (Tauxe, 2007; Kodama, 2012;), and can be attributed to a number of factors such as: non-vertical core penetration, or the recording process of the detrital magnetisation (Turner, 2015). Kodama (2012) highlighted that, for example, deposition on a sloping surface or from moving water can also contribute to inclination shallowing, however the extent of this shallowing is uncertain, but it can undoubtedly reach 10° or more.

The PCA analysis corrected for the core tilt, thus this is unlikely to be the cause of the observed shallow inclinations. Prior to the inclination spike of 1700 years BP, in the 4 – 6 mbsf depth range (corresponding to 2000 – 3000 years BP), reduced, fluctuating values of bulk density, low magnetic susceptibility (Figure 5), and coarser magnetic grain size (Figure 13) can be observed. It is likely, that these changes reflect changes in the magnetic mineralogy and compaction, which in turn influence the inclination profile. Disturbances during coring (as shown by the AMS profiles) could also alter the sensitive sediment fabric, and could introduce errors into the inclination values. The pattern of inclination variation is different from the model outputs in the first and last 500 years of the 2PC1 record, and a converse behaviour is observed.

Generally, the declination profile of 2PC1 shows values higher than those of the compared model outputs for most of the record. One high amplitude swing can be identified at around 2000 years BP, which is very similar to the model outputs. The first and last part of the declination record diverge from the model

outputs – this is likely the result of unwanted section rotations, as identified by the offsets at section breaks between sections 1 and 2, and sections 5 and 6.

Prior to comparison of the relative palaeointensity (RPI) results of the core with model outputs, reliability of the RPI record was assessed. Tauxe and Yamazaki (2009) summarised a number of conditions that ideally should be met in order to achieve meaningful RPI calculations:

- the NRM should be characterised by a well-preserved and stable primary component;
- the sediments should be free of inclination error;
- concentration change of the magnetic minerals over the sedimentary sequence should not exceed one magnitude and the grain size change should also be minimal;
- the sequence should be supported by independent chronology.

The palaeomagnetic record of the 2PC1 core satisfies most of these conditions. A stable and well preserved primary component of the NRM could be identified. Concentration and grain size changes are within one magnitude, and the sequence is supported by an independent timescale. As discussed above, the record appears to suffer from inclination shallowing for the 1000 – 2800 years BP period – the level of uncertainty introduced by this in the RPI record is difficult to assess. Nevertheless, when compared with model outputs, the RPI signal shows remarkably good agreement with the pfm9k.1a and CALS10k.1b model outputs for the past 3000 years. The globally observed (Snowball and Sandgren, 2004; Hong et al., 2013; Bourne et al. 2016) geomagnetic field intensity high at ~3000 years BP can clearly be identified in the RPI record of the 2PC1 core.

The palaeomagnetic secular variation features of core 2PC1 show good correlation with model predictions. A number of centennial to millennial scale features can be identified, which strengthen the reliability of the PSV record.

c. Comparison with Western Arctic palaeomagnetic records

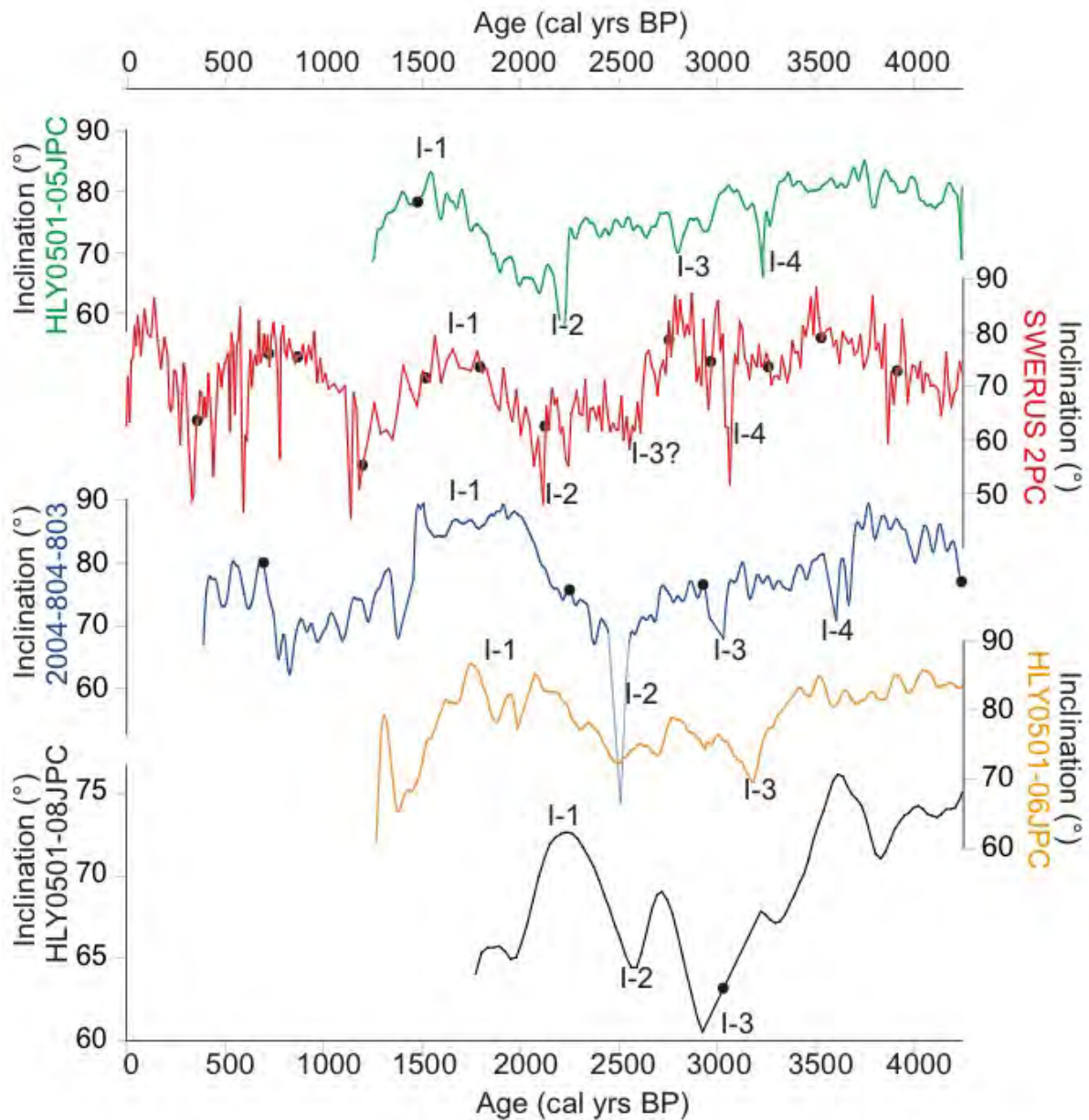


Figure 18: Comparison of magnetic inclination records from the Chukchi- and Beaufort Seas from sediment cores 2PC1, 2004-804-803 and HLY0501-05JPC (Barletta et al. 2008), and HLY0501-06JPC and HLY0501-08JPC (Lisé-Pronovost et al. 2009) on their own chronology. The black markers indicate available radiocarbon dates from the cores and are displayed without error bars. Note that the inclination scales are not identical. For core locations see Figure 2 – marker colours are identical.

Comparison of the ChRM inclination record of 2PC1 with other Western Canadian and Alaskan Arctic palaeomagnetic records from the area (cores 2004-804-803, HLY0501-05JPC, HLY0501-06JPC and JLY0501-08JPC)

reveals a number of common magnetic inclination features (Figure 18). One of the most prominent of these, inclination feature I-1, between 1500–2000 years BP, can be clearly identified in all records, and was first described by Lisé-Pronovost et al. (2009), and by Barletta et al. (2010). Lisé-Pronovost et al. (2009) attributed a mean age of 2030 ± 130 years to this feature, however, the 2PC1 record suggests a mean age of 1740 ± 123 years, which is ~ 100 – 200 years younger than the previously proposed age. The difference is likely to result from differences in the age models. There are three radiocarbon dates available for this period alone for the 2PC1 record, providing a very strong chronological control. Notable inclination minima can be observed at 1150, ~ 2150 (I-2) and ~ 3100 (I-4) years BP, and these features are also readily identifiable in the records of the other cores, however, they consistently appear older in these records. The discrepancies between the ages are not surprising: a summary of available radiocarbon dates for the other cores (Table 2) reveals the scarcity of absolute ages for the 0 – 4500 years BP period, and the range of reservoir corrections applied. Also shown are radiocarbon dates for three cores (MC-14, GCC-19, JPC-16) from the Eastern Chukchi Sea (palaeomagnetic data for these records were not available).

Core	Dated material	AMS 14C age (yrs BP) for the period 0 – 4500 BP	Calibrated age (average cal yrs BP) for the period 0 – 4500 BP	Regional reservoir correction, ΔR (years)
2004-804-803	Yolida myalis Buccinum sp. Shell fragments Shell fragments	1530 ± 40 3000 ± 40 3540 ± 40 4560 ± 40	693 2249 2928 4242	400
HLY0501-05JPC	Thyasira sp.	1930 ± 45	1477	0
HLY0501-06JPC	No dated material for this period	No age for this period	No age for this period	0
HLY0501-08JPC	Bivalve Macoma	3216 ± 37	3030	0
MC-14	Thyasira fragment Thyasira fragment	527 ± 33 1457 ± 34	0 559	Not available
GCC-19	Benthic foraminifera Mollusc Benthic foraminifer	2040 ± 35 3650 ± 40 4270 ± 40	1079 2935 3700	Not available
JPC-16	Bivalve Thyasira fragment	2110 ± 45 4529 ± 41	1159 4036	Not available

Table 2: Radiocarbon dates for cores 2004-804-803, HLY0501-05JPC (Barletta et al. 2008), HLY0501-06JPC, HLY0501-08JPC (Lisé-Pronovost et al. 2009), MC-14, GCC-19, and JPC-16 (Darby et al. 2012; Lund et al. 2016) for the last 4500 years.

Comparison with the declination features of other Western Arctic cores is problematic. None of the cited cores were azimuthally oriented. Therefore, the available declination profiles were relative. Corrections were applied not only for circular values, but for rotations at section breaks as well (Lisé-Pronovost, 2009). These can all introduce large uncertainties, which question the reliability of any meaningful comparison of declination profiles. Therefore, no such comparison was conducted.

Barletta et al. (2008) identified relative palaeointensity highs at 2000 and 4000 years BP in the record of both cores 2004-804-803, and HLY0501-05JPC. The RPI signal of 2PC1 confirms the intensity high at about 2000 years BP (with a duration of approximately 700 years), and the preceding intensity low (Figure 19). However, these RPI features were not as apparent in the RPI signals of HLY-0501-06JPC and -08JPC (Lisé-Pronovost, 2009).

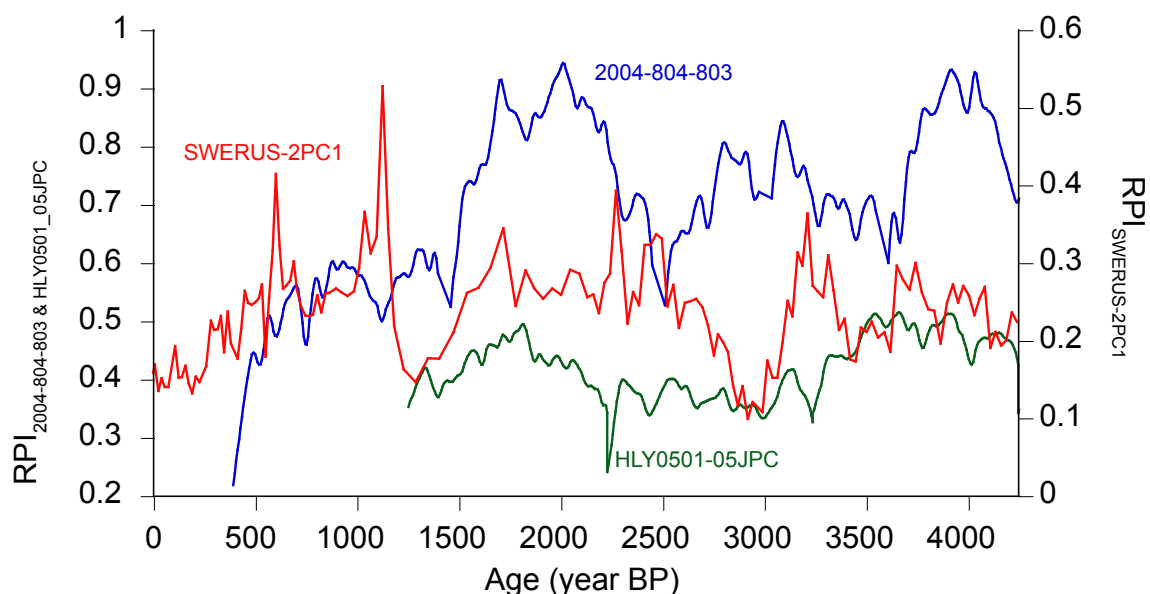


Figure 19: Relative palaeointensities for cores SWERUS-2PC1, 2004-804-803 and HLY0501-05 JPC. Note that the RPI scales are not identical to reflect the differences in the RPI determination methods.

The inclination profile of the 2PC1 core shows millennial-scale trends over the last 4200 years very similar to other palaeomagnetic records available from the area (2004-804-803, HLY0501-05JPC, HLY0501-06JPC and JLY0501-08JPC). Directly comparable centennial-scale fluctuations can also be observed in the inclination record of the cores. This agreement in the inclination variability amongst the records clearly indicates that the 2PC1 core is a good recorder of the palaeomagnetic inclination signal. Supported by a large number of absolute ages, and a firm age-depth model, the PSV record of the core, and in particular its inclination signal, can be utilised to constrain the chronologies of other sequences, which lack independent timescales.

d. Future perspectives

- The study was based on the assumption that the magnetic remanence was carried by magnetite. It is essential that the remanence carrier is identified via microscopy, thermomagnetic experiments or coercivity spectrum analysis. Determining the magnetic mineralogy would also help to clarify the marked concentration and grain size changes observed in the 4 – 6 mbsf depth range.
- There are a number of ways to correct for inclination shallowing – these methods are, however, beyond the scope of the current study. Therefore, correction for inclination errors should be attempted by future research.
- The palaeomagnetic secular variation record of the core was compared with Arctic cores from sites that lie east of Herald Canyon. Records from areas west of Herald Canyon, e. g. from the East Siberian Sea would be beneficial for comparison, in order to construct a more complete picture of the geomagnetic field variability of the region.

7. Conclusions

The presented palaeosecular variation record of the SWERUS-2PC1 core is the first high resolution palaeomagnetic record from the Herald Canyon, Chukchi Sea, spanning the Late Holocene from 4200 years BP to present. The age model of the core is based on 14 radiocarbon dates, providing a robust, independent timescale for the core.

The 2PC1 sedimentary sequence recorded a good quality palaeomagnetic signal: variability in palaeomagnetic inclination and declination conform well to predictions made by time-varying geomagnetic field models, such as A-FM, pfm9k.1a, CALS3K.4e and CALS10K.1b. The RPI signal of 2PC1 reveals centennial - millennial scale changes, which are consistent with changes of Earth's dipole moment as predicted by the field models.

The palaeomagnetic secular variation features of the 2PC1 core are also consistent with the palaeomagnetic inclination and relative palaeointensity profiles of other Western Arctic cores (2004-804-803, HLY0501-05JPC, HLY0501-06JPC and JLY0501-08JPC). The PSV record of 2PC1 provides valuable insights into the local geomagnetic field behaviour for the past 4200 years, including observations for the past 1000 years, which most of the compared Western Arctic records do not sample. The common palaeomagnetic features, coupled with the strong chronological control provided by a robust age-depth model allow the 2PC1 PSV record to be used as a chronological reference tool to tune Western Arctic records that suffer from a lack of independent age control.

Acknowledgements

I would like to thank my MSc Project supervisor Dr Matt O'Regan of the Department of Geological Sciences at Stockholm University. His knowledge and support have been absolutely invaluable for me. I would also like to thank Prof. Ian Snowball at the Department of Earth Sciences, Uppsala University for his valuable feedback. Steffen Wiers of the Department of Earth Sciences, Uppsala University for answering my questions and for his help with palaeomagnetic measurements. Dr Andreas Nilsson and Dr Neil Suttie of the Department of Geology at Lund University for all their help in the Palaeomagnetic Laboratory.

Finally, I would like to thank the Department of Geological Sciences of Stockholm University for the opportunity and funding, which allowed me to undertake this research project.

References

- Archanjo, C. J., Silva, M. G., Castro, J. C., Launeau, P., Trindade, R. I. F., & Macedo, J. W. P. (2006) AMS and grain shape fabric of the Late Palaeozoic diamictites of the Southeastern Parana Basin, Brazil. *Journal of the Geological Society*, 163(1), 95–106.
- Backman, J., Jakobsson, M., Løvlie, R., Polyak, L., & Febo, L. A. (2004) Is the central Arctic Ocean a sediment starved basin? In *Quaternary Science Reviews* (Vol. 23, pp. 1435–1454).
- Barletta, F., St-Onge, G., Channell, J. E. T., Rochon, A., Polyak, L., Darby, D. (2008) High-resolution paleomagnetic secular variation and relative paleointensity records from the western Canadian Arctic: implication for Holocene stratigraphy and geomagnetic field behaviour. *Canadian Journal of Earth Sciences*, 45(11), 1265–1281.
- Barletta, F., St-Onge, G., Channell, J. E. T., & Rochon, A. (2010) Dating of Holocene western Canadian Arctic sediments by matching paleomagnetic secular variation to a geomagnetic field model. *Quaternary Science Reviews*, 29(17–18), 2315–2324.
- Bourne, M. D., Feinberg, J. M., Stafford, T. W., Waters, M. R., Lundelius, E., & Forman, S. L. (2016) High-intensity geomagnetic field “spike” observed at ca. 3000 cal BP in Texas, USA. *Earth and Planetary Science Letters*, 442, 80–92.
- Bradley, R. S. (2015) *Paleoclimatology: reconstructing climates of the Quaternary*. Third edition. Amsterdam, Elsevier.
- Brown, M.C., F. Donadini, A. Nilsson, S. Panovska, U. Frank, K. Korhonen, M. Schuberth, M. Korte and C.G. Constable (2015) GEOMAGIA50.v3: 2. A new paleomagnetic database for lake and marine sediments, *Earth Planets Space* 67:70.
- Chadima, M., Jelinek, V. (2008) Anisoft 4.2 – anisotropy data browser. *Geophys. Geod.*, 38 (Special Issue). 41.
- Channell, J. E. T., & Xuan, C. (2009) Self-reversal and apparent magnetic excursions in Arctic sediments. *Earth and Planetary Science Letters*, 284(1–2), 124–131.
- Chen, H., Sun, W., S., Zhang, H. (1996) Anisotropy of magnetic susceptibility and identification of tilted sediment cores from the Bohai Sea. *Chinese Journal of Oceanology and Limnology*, 14(2), 135–140.
- Clark, D. L., Vincent, J. S., Jones, G. A., & Morris, W. A. (1984) Correlation of marine and continental glacial and interglacial events, Arctic Ocean and Banks Island
- Darby, D.A., Polyak, L. and Jakobsson, M., (2009) The 2005 HOTRAX expedition to the Arctic Ocean. *Global and Planetary Change*, 68(1), pp.1–4.
- Evan, M., Heller, F. (2003) *Environmental Magnetism – Principles and Applications of Enviromagnetics introduction International Geophysics*, 86, 1–I.
- Hong, H., Yu, Y., Lee, C.H., Kim, R.H., Park, J., Doh, S.J., Kim, W., Sung, H., (2013) Globally strong geomagnetic field intensity circa 3000 years ago. *Earth Planet. Sci. Lett.*383, 142–152.

Jakobsson, M., Pearce, C., Cronin, T. M., Backman, J., Anderson, L. G., Barrientos, N., Björk, G., Coxall, H., de Boer, A., Mayer, L. A., Mörth, C.-M., Nilsson, J., Rattray, J. E., Stranne, C., Semilietov, I., and O'Regan, M. (2017) Post-glacial flooding of the Beringia Land Bridge dated to 11,000 cal yrs BP based on new geophysical and sediment records, *Clim. Past Discuss.*, doi:10.5194/cp-2017-11, in review.

Kearey, P., Brooks, M., Hill, I. (2002) *An Introduction to Geophysical Exploration*. Third edition, Oxford, Blackwell Science Ltd.

King, J., Banerjee, J., Marvin, J., Özdemir, Ö. (1982) A comparison of different magnetic methods of determining the relative grain size of magnetite in natural materials: some results from lake sediments. *Earth and Planetary Science Letters*, 59, 404-419.

Kirschwink, J. L. (1980) The least-squares line and plane and the analysis of paleomagnetic data. *Geophysical Journal of the Royal Astronomical Society*, 62, 699 – 718.

Kodama, K. P. (2012) *Paleomagnetism of Sedimentary Rocks: Process and Interpretation*. *Paleomagnetism of Sedimentary Rocks: Process and Interpretation*.

Korte, M. and C. Constable (2011) Improving geomagnetic field reconstructions for 0 – 3ka. *Phys. Earth Planet. Int.*, 188, p. 247-259.

Korte, M., C. Constable, F. Donadini and R. Holme (2011) Reconstructing the Holocene Geomagnetic Field. *Earth Planet Sci. Lett.*, 312, p. 497-505.

Laj, C., Channell, J.E.T., (2007) Geomagnetic excursions. In: Kono, M. (Ed.), *Treatise on Geophysics. Geomagnetism*, vol. 5. Elsevier, Amsterdam, pp. 373-416. Chapter 10.

Lawrence, K. P., Tauxe, L., Staudigel, H., Constable, C. G., Koppers, A., McIntosh, W., Johnson, C. L. (2009) Paleomagnetic field properties at high southern latitude. *Geochemistry, Geophysics, Geosystems*, 10(1).

Licht, A., Hulot, G., Gallet, Y., & Thibault, E. (2013) Ensembles of low degree archeomagnetic field models for the past three millennia. *Physics of the Earth and Planetary Interiors*, 224, 38-67.

Lisé-Pronovost, A., St-Onge, G., Brachfeld, S., Barletta, F., & Darby, D. (2009) Paleomagnetic constraints on the Holocene stratigraphy of the Arctic Alaskan margin. *Global and Planetary Change*, 68(1-2), 85-99.

Løvlie, R., Markussen, B., Sejrup, H. P., & Thiede, J. (1986) Magnetostratigraphy in three Arctic Ocean sediment cores; arguments for geomagnetic excursions within oxygen-isotope stage 2-3. *Physics of the Earth and Planetary Interiors*, 43(2), 173-184.

Lund, S., Keigwin, L., & Darby, D. (2016) Character of Holocene paleomagnetic secular variation in the tangent cylinder: Evidence from the Chukchi Sea. *Physics of the Earth and Planetary Interiors*, 256, 49-58.

Maher, B. Hounslow, M. W. (1999) *Palaeomonsoons II; Magnetic records of aeolian dust in Quaternary sediments of the Indian Ocean*. In Maher, B. A. and Thompson, R. (eds) *Quaternary Climates, Environments and Magnetism*. Cambridge University Press.

- Mazaud, A. (2005) User-friendly software for vector analysis of the magnetization of long sediment cores. *Geochemistry, Geophysics, Geosystems*, 6(12).
- Nilsson, A., Holme, R., Korte, M., Suttie, N., & Hill, M. (2014) Reconstructing holocene geomagnetic field variation: New methods, models and implications. *Geophysical Journal International*, 198(1), 229–248.
- O'Regan, M., King, J., Backman, J., Jakobsson, M., Palike, H., Moran, K., Heil, C., Sakamoto, T., Cronin, T.M., Jordan, R.W., (2008) Constraints on the Pleistocene chronology of sediments from the Lomonosov Ridge. *Paleoceanography* 23, PA1S19.
- O'Regan, M., Preto, P., Stranne, C., Jakobsson, M., Koshurnikov, A. (2016) Surface heat flow measurements from the East Siberian continental slope and southern Lomonosov Ridge, Arctic Ocean. *Geochemistry, Geophysics, Geosystems*, 17.
- Pearce, C., Varhelyi, A., Wastegård, S., Muschitiello, F., Barrientos, N., O'Regan, M., Jakobsson, M. (2017) The 3.6ka Aniakchak tephra in the Arctic Ocean: A constraint on the Holocene radiocarbon reservoir age in the Chukchi Sea. *Climate of the Past*, 13(4), 303–316.
- Pickart, R. S., Pratt, L. J., Torres, D. J., Whitedge, T. E., Proshutinsky, A. Y., Aagaard, K., Dail, H. J. (2010) Evolution and dynamics of the flow through Herald Canyon in the western Chukchi Sea. *Deep Sea Research Part II: Topical Studies in Oceanography*, 57(1), 5–26.
- Roberts, A. P., Tauxe, L., Heslop, D. (2013) Magnetic paleointensity stratigraphy and high-resolution Quaternary geochronology: Successes and future challenges. *Quaternary Science Reviews*.
- Rothwell RG, Croudace IW (2015) Twenty years of XRF core scanning marine sediments: What do geochemical proxies tell us? In: Croudace IW, Rothwell RG (eds) *Micro-XRF Studies of Sediment Cores: Applications of a Non-Destructive Tool for the Environmental Sciences*. Dordrecht: Springer, pp. 25–102
- Sagnotti, L. (2013) Demagnetization Analysis in Excel (DAIE). An open source workbook in Excel for viewing and analyzing demagnetization data from paleomagnetic discrete samples and u-channels. *Annals of Geophysics*, 56(1).
- Snowball, I., & Sandgren, P. (2004) Geomagnetic field intensity changes in Sweden between 9000 and 450 cal BP: Extending the record of “archaeomagnetic jerks” by means of lake sediments and the pseudo-Thellier technique. *Earth and Planetary Science Letters*, 227(3–4), 361–376.
- Spall, M. A. (2007) Circulation and water mass transformation in a model of the Chukchi Sea. *Journal of Geophysical Research: Oceans*, 112(5).
- Stoner, J. S., & St-Onge, G. (2007) Chapter Three Magnetic Stratigraphy in Paleooceanography: Reversals, Excursions, Paleointensity, and Secular Variation. *Developments in Marine Geology*.
- St-Onge, G., Stoner, J. S. (2011) Paleomagnetism near the North Magnetic Pole. *Oceanography* vol. 24.
- Tauxe, L. (1993). *Sedimentary records of relative paleointensity of the geomagnetic field: Theory and practice*. *Reviews of Geophysics*.

Tauxe, L. (2010) *Essentials of Paleomagnetism*. University of California Press.

Tauxe, L., & Yamazaki, T. (2007). *Paleointensities*. In *Treatise on Geophysics* (Vol. 5, pp. 509–563).

Turner, G. M., Howarth, J. D., de Gelder, G. I. N. O., & Fitzsimons, S. J. (2015) A new high-resolution record of Holocene geomagnetic secular variation from New Zealand. *Earth and Planetary Science Letters*, 430, 296–307.

Valet, J.-P. (2003) Time variations in geomagnetic intensity. *Reviews of Geophysics*, 41(1), 1004.

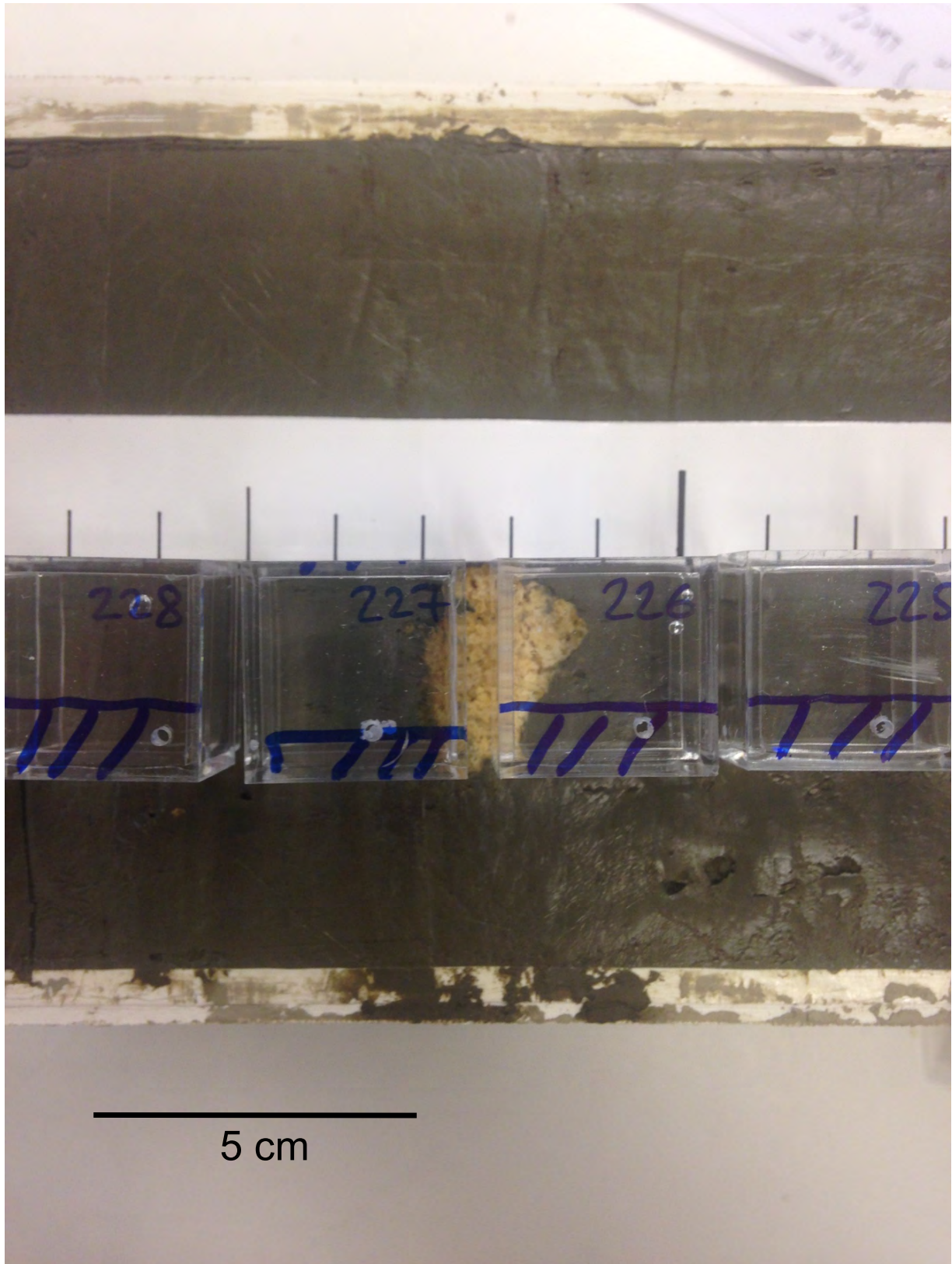
Wegner, C., Bennett, K.E., de Vernal, A., Forwick, M., Fritz, M., Heikkilä, M., Lacka, M., Lantuit, H., Laska, M., Moskalik, M., O'Regan, M., Pawłowska, J., Promińska, A., Rachold, V., Vonk, J. E., Werner, K., (2015) Variability in transport of terrigenous material on the shelves and the deep Arctic Ocean during the Holocene. *Polar Research*, 34, 24964.

Weingartner, T., Aagaard, K., Woodgate, R., Danielson, S., Sasaki, Y., & Cavalieri, D. (2005) Circulation on the north central Chukchi Sea shelf. *Deep-Sea Research II*, 52, 3150–3174.

Xuan, C., & Channell, J. E. T. (2010) Origin of apparent magnetic excursions in deep-sea sediments from Mendeleev-Alpha Ridge, Arctic Ocean. *Geochemistry, Geophysics, Geosystems*, 11(2).

Zijderveld, J.D.A. (1967) A.C. demagnetization of rocks: analysis of results. In D.W. Collinson, K.M. Creer, S.K. Runcorn (Eds.), *Methods in Paleomagnetism*, Elsevier, Amsterdam (1967), pp. 254–286.

Appendices
Appendix I.



Nodule found at 5.87 mbsf in the 2PC1 core. Palaeomagnetic sample boxes 226 and 227 were not filled.

Appendix II.

Sample number	Top Depth (cm)	Mass (g)	Sample number	Top Depth (cm)	Mass (g)
1-001	0.0	13.196	2-039	0.0	13.349
1-002	2.6	13.330	2-040	3.1	13.451
1-003	5.1	13.101	2-041	5.6	13.419
1-004	7.6	12.167	2-042	8.2	13.278
1-005	10.1	12.344	2-043	10.6	13.287
1-006	12.4	12.567	2-044	13.1	13.107
1-007	14.9	13.043	2-045	15.6	11.770
1-008	17.5	12.834	2-046	18.1	13.226
1-009	19.8	12.577	2-047	20.6	13.389
1-010	22.6	13.140	2-048	23.0	13.474
1-011	25.2	13.336	2-049	25.4	13.480
1-012	27.7	13.310	2-050	27.9	13.647
1-013	30.1	13.136	2-051	30.4	13.591
1-014	32.7	13.350	2-052	32.9	13.365
1-015	35.2	13.554	2-053	35.5	13.601
1-016	37.6	13.201	2-054	37.9	13.416
1-017	40.4	13.400	2-055	40.4	13.511
1-018	42.9	12.988	2-056	42.9	13.351
1-019	45.4	13.489	2-057	45.4	13.575
1-020	47.9	13.130	2-058	47.8	13.464
1-021	50.3	13.270	2-059	50.5	13.447
1-022	52.9	13.374	2-060	53.1	13.482
1-023	55.5	12.745	2-061	55.6	13.502
1-024	58.1	13.082	2-062	58.2	13.538
1-025	60.6	13.397	2-063	60.7	13.646
1-026	63.2	13.279	2-064	63.3	13.826
1-027	65.7	13.481	2-065	65.7	13.374
1-028	68.3	13.374	2-066	68.3	13.753
1-029	70.8	12.737	2-067	71.0	13.626
1-030	73.5	12.770	2-068	73.6	13.560
1-031	75.4	12.601	2-069	76.1	13.615
1-032	78.6	13.175	2-070	78.6	13.663
1-033	81.2	13.152	2-071	81.1	13.828
1-034	83.8	13.399	2-072	83.7	13.716
1-035	86.5	13.030	2-073	86.4	13.828
1-036	89.0	13.279	2-074	89.1	13.523
1-037	91.6	13.325	2-075	91.6	13.605
1-038	94.4	13.469	2-076	94.2	13.704
			2-077	96.7	13.656
			2-078	99.4	13.537
			2-079	101.9	13.400
			2-080	104.5	13.463
			2-081	107.0	13.523
			2-082	109.5	13.321
			2-083	112.1	13.357
			2-084	114.6	13.574
			2-085	117.3	13.386
			2-086	119.9	13.437
			2-087	122.5	13.916
			2-088	125.2	13.777
			2-089	127.8	13.863
			2-090	130.4	13.581
			2-091	133.2	13.570
			2-092	135.8	13.625
			2-093	138.4	13.958
			2-094	141.0	13.754
			2-095	143.8	13.937
			2-096	146.2	13.592
			2-097	148.0	13.412

Sample number	Top Depth (cm)	Mass (g)	Sample number	Top Depth (cm)	Mass (g)
3-099	2.7	13.512	4-154	0.0	14.098
3-100	5.4	13.599	4-155	2.5	13.961
3-101	8.0	13.663	4-156	5.2	14.011
3-102	10.7	13.804	4-157	7.8	13.899
3-103	13.3	13.720	4-158	10.4	13.715
3-104	15.8	13.822	4-159	13.4	14.158
3-105	18.5	13.323	4-160	15.8	14.169
3-106	20.0	13.802	4-161	18.4	14.034
3-107	23.7	13.820	4-162	21.1	14.081
3-108	26.4	13.934	4-163	23.9	14.002
3-109	28.9	13.722	4-164	26.5	14.240
3-110	31.6	13.831	4-165	29.1	14.081
3-111	34.3	13.908	4-166	31.9	14.217
3-112	37.0	13.846	4-167	34.6	14.247
3-113	39.6	13.784	4-168	37.2	14.182
3-114	42.6	13.981	4-169	40.0	14.096
3-115	44.9	13.665	4-170	42.5	14.191
3-116	47.5	13.708	4-171	45.2	14.127
3-117	50.0	13.774	4-172	47.9	13.934
3-118	52.9	13.772	4-173	50.6	14.020
3-119	55.4	13.877	4-174	53.2	14.069
3-120	58.2	13.716	4-175	55.9	13.938
3-121	61.0	13.721	4-176	58.5	13.857
3-122	63.5	13.621	4-177	61.3	14.026
3-123	66.1	13.595	4-178	64.0	14.096
3-124	69.0	13.585	4-179	66.9	14.242
3-125	71.5	13.305	4-180	69.4	14.229
3-126	74.1	13.871	4-181	72.1	14.232
3-127	76.9	13.608	4-182	74.9	14.157
3-128	79.5	13.741	4-183	77.4	14.115
3-129	82.2	13.803	4-184	80.1	14.090
3-130	84.9	13.693	4-185	82.8	13.893
3-131	87.5	14.028	4-186	85.4	14.209
3-132	90.2	13.871	4-187	88.2	14.258
3-133	92.9	13.581	4-188	90.9	14.131
3-134	95.5	13.675	4-189	93.5	14.142
3-135	98.0	13.760	4-190	96.0	13.999
3-136	100.2	14.246	4-191	98.9	14.098
3-137	103.6	14.108	4-192	101.3	13.935
3-138	106.5	14.084	4-193	104.1	14.092
3-139	109.1	14.071	4-194	106.7	14.146
3-140	112.2	13.995	4-195	109.5	14.213
3-141	114.5	14.369	4-196	112.1	14.070
3-142	117.2	14.191	4-197	114.8	14.095
3-143	119.9	14.102	4-198	117.5	14.033
3-144	122.5	13.857	4-199	120.2	14.415
3-145	125.3	13.984	4-200	122.9	14.233
3-146	127.9	14.100	4-201	125.6	14.169
3-147	130.6	14.154	4-202	128.2	14.029
3-148	133.3	13.904	4-203	131.0	14.048
3-149	136.1	14.155	4-204	133.8	14.016
3-150	138.5	14.130	4-205	136.4	14.182
3-151	141.3	13.903	4-206	139.3	14.255
3-152	143.9	13.985	4-207	142.0	14.180
3-153	146.7	13.900	4-208	144.9	14.318
			4-209	147.5	14.068

Sample number	Top Depth (cm)	Mass (g)	Sample number	Top Depth (cm)	Mass (g)
5-210	0.0	14.238	6-261	0.0	13.608
5-211	2.5	14.620	6-262	2.5	13.848
5-212	5.0	14.237	6-263	5.0	13.770
5-213	7.5	14.423	6-264	7.5	13.746
5-214	10.0	14.186	6-265	10.0	13.635
5-215	12.5	14.434	6-266	12.5	13.640
5-216	15.0	14.285	6-267	15.0	13.822
5-217	17.5	14.161	6-268	17.5	13.637
5-218	20.0	13.991	6-269	20.0	14.010
5-219	22.5	14.138	6-270	22.5	13.880
5-220	25.0	14.173	6-271	25.0	14.065
5-221	27.5	14.431	6-272	27.5	13.814
5-222	30.0	14.691	6-273	30.0	14.158
5-223	32.5	14.816	6-274	32.5	14.211
5-224	35.0	14.694	6-275	35.0	14.190
5-225	37.5	14.613	6-276	37.5	14.086
5-226	40.0	-	6-277	40.0	14.000
5-227	42.5	-	6-278	42.5	13.995
5-228	45.0	14.989	6-279	45.0	14.003
5-229	47.5	14.331	6-280	47.5	14.099
5-230	50.0	14.471	6-281	50.0	13.880
5-231	52.5	14.333	6-282	52.5	13.802
5-232	55.0	14.491	6-283	55.0	13.880
5-233	57.5	14.316	6-284	57.5	13.933
5-234	60.0	14.439	6-285	60.0	13.922
5-235	62.5	14.443	6-286	62.5	14.235
5-236	65.0	14.401	6-287	65.0	14.208
5-237	67.5	14.357	6-288	67.5	14.297
5-238	70.0	14.425	6-289	70.0	14.127
5-239	72.5	14.318	6-290	72.5	14.098
5-240	75.0	14.131	6-291	75.0	14.037
5-241	77.5	14.273	6-292	77.5	13.592
5-242	80.0	14.194	6-293	80.0	14.203
5-243	82.5	14.243	6-294	82.5	14.353
5-244	85.0	14.191	6-295	85.0	14.173
5-245	87.5	14.172	6-296	87.5	14.296
5-246	90.0	14.337	6-297	90.0	14.376
5-247	92.5	14.250	6-298	92.5	14.308
5-248	95.0	14.286	6-299	95.0	14.498
5-249	97.5	14.323	6-300	97.5	14.425
5-250	100.0	14.351	6-301	100.0	14.413
5-251	102.5	14.327	6-302	102.5	14.325
5-252	105.0	14.358	6-303	105.0	14.482
5-253	107.5	14.266	6-304	107.5	14.347
5-254	110.0	14.278	6-305	110.0	14.387
5-255	112.5	14.134	6-306	112.5	14.279
5-256	115.0	14.174	6-307	115.0	14.318
5-257	117.5	14.263	6-308	117.5	14.316
5-258	120.0	13.981	6-309	120.0	14.247
5-259	122.5	13.942	6-310	122.5	14.076
5-260	125.0	14.089	6-311	125.0	14.172
			6-312	127.5	14.271
			6-313	130.0	14.389
			6-314	132.5	14.414
			6-315	135.0	14.267
			6-316	137.5	14.234
			6-317	140.0	14.231
			6-318	142.5	14.258
			6-319	145.0	14.294
			6-320	147.5	14.137

Appendix III.

Sample ID	Core depth mid (m bsf)	Age (cal yrs BP)	Decl PCA (°)	Decl PCA - adjusted (°)	Incl PCA (°)	MAD (°)	[Min Step for FIT]	[Max Step for FIT]	[NStep for FIT]	NRM Intensity (A/m)	MDF AF (Oe)
SWE2PC_001_NRM	0.011	-42.3	16.8	16.8	31.8	3.0	200	800	7	1.58E-01	409.0
SWE2PC_002_NRM	0.037	-35.6	26.5	26.5	56.7	2.6	200	800	7	1.80E-01	403.7
SWE2PC_003_NRM	0.062	-29.3	25.1	25.1	59.1	2.1	200	800	7	1.05E-01	446.9
SWE2PC_004_NRM	0.087	-22.9	16.3	16.3	61.7	2.0	200	800	7	1.11E-01	382.4
SWE2PC_005_NRM	0.112	-16.1	38.3	38.3	47.5	2.9	200	800	7	1.11E-01	366.0
SWE2PC_006_NRM	0.135	-8.5	39.8	39.8	69.7	1.5	200	800	7	1.14E-01	418.5
SWE2PC_007_NRM	0.16	-0.3	17.2	17.2	62.1	1.4	200	800	7	1.15E-01	397.2
SWE2PC_008_NRM	0.186	8.3	26.5	26.5	71.1	2.0	200	800	7	1.67E-01	390.1
SWE2PC_009_NRM	0.209	15.9	15.9	15.9	62.8	2.1	200	800	7	1.49E-01	362.6
SWE2PC_010_NRM	0.237	25.1	59.2	59.2	74.3	2.0	200	800	10	1.42E-01	407.4
SWE2PC_011_NRM	0.263	33.7	53.4	53.4	74.9	1.5	200	800	7	1.26E-01	407.4
SWE2PC_012_NRM	0.288	41.9	60.7	60.7	80.6	1.4	200	800	7	1.88E-01	363.0
SWE2PC_013_NRM	0.312	49.8	102.7	102.7	77.2	1.0	200	800	7	1.74E-01	370.7
SWE2PC_014_NRM	0.338	58.4	103.5	103.5	82.5	0.8	200	800	7	1.47E-01	418.6
SWE2PC_015_NRM	0.363	66.6	123.7	123.7	79.4	1.8	200	800	7	2.24E-01	357.8
SWE2PC_016_NRM	0.387	74.6	52.2	52.2	75.2	1.1	200	800	7	1.65E-01	383.3
SWE2PC_018_NRM	0.44	92	73.1	73.1	83.8	1.1	200	800	7	1.69E-01	389.9
SWE2PC_020_NRM	0.49	108.5	92.9	92.9	79.2	1.3	200	800	7	2.15E-01	416.8
SWE2PC_022_NRM	0.54	125	86.2	86.2	78.6	1.5	200	800	7	1.59E-01	423.4
SWE2PC_024_NRM	0.592	142.1	86.6	86.6	85.9	0.7	200	800	7	1.40E-01	455.5
SWE2PC_026_NRM	0.643	158.9	129.7	129.7	77.9	0.5	200	800	7	1.79E-01	437.6
SWE2PC_028_NRM	0.694	175.7	127.7	127.7	72.6	1.4	200	800	7	1.93E-01	381.1
SWE2PC_030_NRM	0.746	192.9	129.7	129.7	78.5	1.4	200	800	10	1.31E-01	462.2
SWE2PC_032_NRM	0.797	209.7	160.7	160.7	75.4	1.8	200	800	7	1.71E-01	443.4
SWE2PC_033_NRM	0.823	218.2	104.2	104.2	66.1	1.5	200	800	7	1.62E-01	384.3
SWE2PC_034_NRM	0.849	226.8	127.6	127.6	64.7	0.9	200	800	7	1.65E-01	455.0
SWE2PC_035_NRM	0.876	235.7	64.6	64.6	65.7	1.7	200	800	7	1.44E-01	444.1
SWE2PC_036_NRM	0.901	243.9	149.6	149.6	72.4	1.2	200	800	7	1.75E-01	438.7
SWE2PC_037_NRM	0.927	252.5	130.2	130.2	71.9	1.1	200	800	7	1.97E-01	415.3
SWE2PC_038_NRM	0.955	261.7	92.3	92.3	68.7	1.1	200	800	7	1.89E-01	436.5
SWE2PC_039_NRM	0.991	273.6	323.9	-36.1	58.5	0.9	200	800	7	2.48E-01	453.1
SWE2PC_040_NRM	1.022	283.8	330.1	-29.9	67.9	0.8	200	800	7	2.54E-01	459.8
SWE2PC_041_NRM	1.047	292.1	335.3	-24.7	73.6	0.8	200	800	7	2.00E-01	463.8
SWE2PC_042_NRM	1.073	300.6	328.4	-31.6	71.4	0.6	200	800	7	2.24E-01	469.3
SWE2PC_043_NRM	1.097	308.5	353.3	-6.7	65.2	0.6	200	800	7	1.39E-01	439.4
SWE2PC_044_NRM	1.122	316.8	349.5	-10.5	58.6	0.9	200	800	7	2.17E-01	458.8
SWE2PC_045_NRM	1.147	325	357.9	-2.1	54.0	0.6	200	800	7	1.51E-01	461.9
SWE2PC_046_NRM	1.172	333.3	335.8	-24.2	47.9	0.6	200	800	7	1.73E-01	424.7
SWE2PC_047_NRM	1.197	341.5	346.6	-13.4	49.0	1.0	200	800	7	1.56E-01	444.9
SWE2PC_048_NRM	1.221	349.4	345.8	-14.2	56.6	0.6	200	800	7	1.36E-01	419.4
SWE2PC_049_NRM	1.245	357.3	347.3	-12.7	62.3	1.3	200	800	7	2.06E-01	434.6
SWE2PC_050_NRM	1.27	365.7	336.4	-23.6	64.0	0.8	200	800	10	2.58E-01	437.0
SWE2PC_051_NRM	1.295	374	11.0	11.0	68.5	0.7	200	800	7	2.00E-01	450.2
SWE2PC_052_NRM	1.32	382.3	329.8	-30.2	68.1	0.8	200	800	7	2.00E-01	455.5
SWE2PC_053_NRM	1.346	391	350.5	-9.5	63.4	1.0	200	800	7	1.18E-01	434.0
SWE2PC_054_NRM	1.37	399	333.1	-26.9	67.2	0.8	200	800	7	2.50E-01	447.8
SWE2PC_055_NRM	1.395	407.4	345.0	-15.0	63.8	0.6	200	800	7	2.38E-01	452.2
SWE2PC_056_NRM	1.42	415.7	356.8	-3.2	71.7	2.0	200	800	7	1.43E-01	422.2
SWE2PC_057_NRM	1.445	424.1	335.1	-24.9	66.9	0.9	200	800	7	1.38E-01	439.1
SWE2PC_058_NRM	1.469	432.1	336.2	-23.8	62.5	0.9	200	800	7	2.11E-01	442.2
SWE2PC_059_NRM	1.496	441.1	350.2	-9.8	52.7	0.8	200	800	7	2.05E-01	433.3
SWE2PC_060_NRM	1.522	449.7	347.6	-12.4	60.2	1.5	200	800	7	2.34E-01	454.7
SWE2PC_061_NRM	1.547	458.1	335.1	-24.9	66.9	1.0	200	800	7	1.98E-01	440.3
SWE2PC_062_NRM	1.573	466.8	326.9	-33.1	73.6	0.4	200	800	7	2.05E-01	426.4
SWE2PC_063_NRM	1.598	475.1	348.1	-11.9	72.1	0.6	200	800	7	2.09E-01	439.5
SWE2PC_064_NRM	1.624	483.8	334.6	-25.4	69.3	1.7	200	800	7	2.39E-01	409.9
SWE2PC_065_NRM	1.648	491.8	345.5	-14.5	72.0	1.0	200	800	7	1.82E-01	424.8
SWE2PC_066_NRM	1.674	500.5	336.7	-23.3	73.6	0.8	200	800	7	2.11E-01	440.7
SWE2PC_068_NRM	1.727	518.1	4.5	4.5	75.6	0.9	200	800	7	1.65E-01	427.9
SWE2PC_069_NRM	1.752	526.5	5.9	5.9	60.9	2.3	200	800	7	2.30E-01	385.7
SWE2PC_070_NRM	1.777	534.8	341.9	-18.1	79.3	0.6	200	800	10	2.27E-01	379.6
SWE2PC_071_NRM	1.802	543.2	349.3	-10.7	76.9	0.8	200	800	7	1.56E-01	399.9
SWE2PC_072_NRM	1.828	551.8	344.1	-15.9	64.2	1.7	200	800	7	1.42E-01	411.5
SWE2PC_073_NRM	1.855	560.8	346.2	-13.8	77.0	0.6	200	800	7	2.13E-01	397.2
SWE2PC_074_NRM	1.882	569.8	349.3	-10.7	78.3	1.1	200	800	7	1.65E-01	399.3

SWE2PC_075_NRM	1.907	578.2	352.4	-7.6	84.1	1.4	200	800	7	2.00E-01	380.8
SWE2PC_076_NRM	1.933	586.9	358.5	-1.5	58.9	2.1	200	800	7	2.08E-01	429.2
SWE2PC_077_NRM	1.958	595.2	5.8	5.8	45.9	4.2	200	800	7	2.43E-01	454.4
SWE2PC_078_NRM	1.985	604.2	357.4	-2.6	60.1	3.1	200	800	7	2.27E-01	425.2
SWE2PC_079_NRM	2.01	612.6	2.1	2.1	59.1	1.6	200	800	7	2.62E-01	375.7
SWE2PC_080_NRM	2.036	621.2	348.1	-11.9	69.5	1.2	200	800	7	1.61E-01	409.8
SWE2PC_081_NRM	2.061	629.6	0.2	0.2	76.1	1.0	200	800	7	1.68E-01	402.9
SWE2PC_082_NRM	2.086	637.9	348.5	-11.5	69.4	1.2	200	800	7	1.37E-01	407.1
SWE2PC_083_NRM	2.112	646.6	0.4	0.4	73.8	0.9	200	800	7	9.74E-02	397.5
SWE2PC_084_NRM	2.137	654.9	8.6	8.6	75.1	1.5	200	800	7	1.36E-01	400.5
SWE2PC_085_NRM	2.164	663.9	344.9	-15.1	73.5	0.8	200	800	7	1.66E-01	363.1
SWE2PC_086_NRM	2.19	672.6	344.4	-15.6	81.7	1.4	200	800	7	1.29E-01	408.2
SWE2PC_087_NRM	2.216	681.3	341.2	-18.8	73.9	0.5	200	800	7	1.71E-01	376.7
SWE2PC_088_NRM	2.243	690.3	351.0	-9.0	75.1	1.0	200	800	7	1.52E-01	393.1
SWE2PC_089_NRM	2.269	699	340.5	-19.5	79.1	0.9	200	800	7	1.93E-01	363.4
SWE2PC_090_NRM	2.295	707.6	345.7	-14.3	75.6	0.7	200	800	10	2.11E-01	389.2
SWE2PC_091_NRM	2.323	717	15.8	15.8	78.8	1.4	200	800	7	1.78E-01	423.2
SWE2PC_092_NRM	2.349	726.9	8.6	8.6	73.1	2.3	200	800	7	1.90E-01	402.7
SWE2PC_093_NRM	2.375	737.4	359.5	-0.5	78.9	0.4	200	800	7	2.09E-01	401.6
SWE2PC_094_NRM	2.401	747.8	357.1	-2.9	81.3	0.9	200	800	7	1.89E-01	425.8
SWE2PC_095_NRM	2.429	759.1	2.7	2.7	76.8	0.7	200	800	7	1.68E-01	441.8
SWE2PC_096_NRM	2.453	768.7	344.3	-15.7	71.3	0.7	200	800	7	1.71E-01	419.0
SWE2PC_097_NRM	2.479	779.2	357.8	-2.2	55.9	0.9	200	800	7	1.12E-01	428.3
SWE2PC_098_NRM	2.491	784	345.8	-14.2	78.3	0.8	200	800	7	2.06E-01	394.2
SWE2PC_099_NRM	2.518	794.8	22.3	22.3	80.7	1.5	200	800	7	1.53E-01	412.3
SWE2PC_100_NRM	2.545	805.7	19.1	19.1	75.9	1.1	200	800	7	2.06E-01	417.8
SWE2PC_101_NRM	2.571	816.1	17.1	17.1	74.8	0.8	200	800	7	1.77E-01	419.0
SWE2PC_102_NRM	2.598	827	29.0	29.0	78.3	1.9	200	800	7	2.07E-01	414.5
SWE2PC_103_NRM	2.624	837.4	17.3	17.3	76.1	0.7	200	800	7	1.61E-01	426.9
SWE2PC_104_NRM	2.649	847.4	17.0	17.0	75.3	1.0	200	800	7	2.07E-01	407.3
SWE2PC_105_NRM	2.676	858.3	6.1	6.1	73.6	1.5	200	800	7	1.53E-01	385.4
SWE2PC_106_NRM	2.691	864.3	7.1	7.1	75.1	1.6	200	800	7	1.50E-01	399.0
SWE2PC_107_NRM	2.728	883.6	21.2	21.2	75.0	0.8	200	800	7	1.46E-01	422.3
SWE2PC_108_NRM	2.755	898.1	5.9	5.9	77.1	1.4	200	800	7	1.85E-01	370.5
SWE2PC_109_NRM	2.78	911.5	15.0	15.0	73.6	1.3	200	800	7	1.52E-01	387.1
SWE2PC_110_NRM	2.807	926	22.3	22.3	76.9	1.9	200	800	10	1.72E-01	364.2
SWE2PC_111_NRM	2.834	940.4	17.4	17.4	70.1	7.8	200	800	7	1.45E-01	335.5
SWE2PC_112_NRM	2.861	954.9	29.5	29.5	79.6	1.5	200	800	7	1.34E-01	391.1
SWE2PC_113_NRM	2.887	968.9	156.8	156.8	70.0	5.3	200	800	7	1.35E-01	207.3
SWE2PC_114_NRM	2.917	985	4.3	4.3	74.5	1.0	200	800	7	1.47E-01	347.5
SWE2PC_115_NRM	2.94	997.3	161.7	161.7	70.3	3.8	200	800	7	1.18E-01	215.1
SWE2PC_116_NRM	2.966	1011.2	4.9	4.9	71.7	2.0	200	800	7	1.04E-01	347.1
SWE2PC_117_NRM	2.991	1024.6	153.1	153.1	68.9	5.2	200	800	7	1.12E-01	208.1
SWE2PC_118_NRM	3.02	1040.2	350.1	-9.9	49.6	2.6	200	800	7	1.13E-01	395.3
SWE2PC_119_NRM	3.045	1053.6	157.7	157.7	69.8	4.2	200	800	7	9.91E-02	198.4
SWE2PC_120_NRM	3.073	1068.6	355.3	-4.7	47.9	2.4	200	800	7	9.84E-02	397.4
SWE2PC_121_NRM	3.101	1083.6	152.5	152.5	68.2	6.9	200	800	7	5.28E-02	198.3
SWE2PC_122_NRM	3.126	1097	358.3	-1.7	33.6	2.6	200	800	7	5.56E-02	233.3
SWE2PC_123_NRM	3.152	1111	167.2	167.2	69.5	4.7	200	800	7	6.11E-02	187.2
SWE2PC_124_NRM	3.181	1126.5	351.3	-8.7	34.4	2.9	200	800	7	4.37E-02	369.3
SWE2PC_125_NRM	3.206	1139.9	111.5	111.5	44.7	9.2	200	800	7	4.09E-02	171.4
SWE2PC_126_NRM	3.232	1153.9	18.6	18.6	68.2	3.1	200	800	7	5.33E-02	285.4
SWE2PC_127_NRM	3.26	1168.9	135.7	135.7	65.3	9.1	200	800	7	7.14E-02	97.2
SWE2PC_128_NRM	3.286	1182.8	333.9	-26.1	50.2	2.9	200	800	7	5.37E-02	354.7
SWE2PC_129_NRM	3.313	1199.1	352.4	-7.6	54.3	2.3	200	800	7	6.92E-02	351.1
SWE2PC_130_NRM	3.34	1229.8	24.8	24.8	60.0	2.2	200	800	10	5.73E-02	370.6
SWE2PC_131_NRM	3.366	1259.4	28.4	28.4	66.3	2.7	200	800	7	1.05E-01	304.9
SWE2PC_132_NRM	3.393	1290.1	18.6	18.6	60.6	1.6	200	800	7	7.50E-02	331.6
SWE2PC_133_NRM	3.42	1320.8	46.5	46.5	61.2	3.2	200	800	7	4.67E-02	238.9
SWE2PC_134_NRM	3.446	1350.4	347.0	-13.0	59.4	2.3	200	800	7	9.46E-02	356.6
SWE2PC_135_NRM	3.471	1378.8	17.1	17.1	65.1	1.6	200	800	7	1.19E-01	388.2
SWE2PC_136_NRM	3.493	1403.9	3.9	3.9	73.3	2.0	200	800	7	1.17E-01	409.3
SWE2PC_137_NRM	3.527	1442.5	351.1	-8.9	68.8	0.9	200	800	7	1.45E-01	426.9
SWE2PC_138_NRM	3.556	1475.5	351.8	-8.2	65.7	1.5	200	800	7	1.73E-01	410.3
SWE2PC_139_NRM	3.582	1505.1	8.0	8.0	72.2	1.7	200	800	7	1.59E-01	440.8
SWE2PC_140_NRM	3.613	1540.4	1.5	1.5	70.1	0.9	200	800	7	1.84E-01	438.2
SWE2PC_141_NRM	3.636	1566.5	46.7	46.7	78.8	0.6	200	800	7	1.89E-01	391.0
SWE2PC_142_NRM	3.663	1597.3	17.1	17.1	70.0	1.5	200	800	7	1.46E-01	418.2
SWE2PC_143_NRM	3.69	1628	39.1	39.1	74.3	1.5	200	800	7	1.98E-01	341.4

SWE2PC_144_NRM	3.716	1657.6	29.9	29.9	76.3	1.2	200	800	7	1.17E-01	372.0
SWE2PC_145_NRM	3.744	1689.4	30.2	30.2	72.9	3.1	200	800	7	1.07E-01	309.4
SWE2PC_146_NRM	3.77	1719	28.6	28.6	72.7	1.7	200	800	7	1.09E-01	272.8
SWE2PC_147_NRM	3.797	1749.7	31.0	31.0	72.3	2.8	200	800	7	4.62E-02	308.9
SWE2PC_148_NRM	3.824	1780.4	69.4	69.4	76.0	6.1	200	800	7	8.19E-02	91.7
SWE2PC_149_NRM	3.852	1807.2	46.5	46.5	72.0	3.8	200	800	7	4.29E-02	224.3
SWE2PC_150_NRM	3.876	1827.3	89.9	89.9	72.8	3.2	200	800	10	7.05E-02	130.1
SWE2PC_151_NRM	3.904	1850.7	68.7	68.7	69.5	2.5	200	800	7	7.51E-02	96.9
SWE2PC_152_NRM	3.93	1872.5	74.6	74.6	66.2	3.6	200	800	7	8.88E-02	88.0
SWE2PC_153_NRM	3.958	1895.9	54.0	54.0	64.9	3.7	200	800	7	7.09E-02	85.1
SWE2PC_154_NRM	3.981	1915.2	61.9	61.9	72.7	2.5	200	800	7	4.65E-02	194.4
SWE2PC_155_NRM	4.006	1936.1	70.9	70.9	66.4	3.2	200	800	7	6.15E-02	111.7
SWE2PC_156_NRM	4.033	1958.7	72.1	72.1	62.8	6.3	200	800	7	8.24E-02	77.9
SWE2PC_157_NRM	4.059	1980.5	83.9	83.9	68.7	6.7	200	800	7	7.82E-02	80.0
SWE2PC_158_NRM	4.085	2002.3	100.6	100.6	60.2	5.8	200	800	7	7.21E-02	84.9
SWE2PC_159_NRM	4.115	2027.4	84.0	84.0	65.5	3.8	200	800	7	6.47E-02	106.3
SWE2PC_160_NRM	4.139	2047.5	78.0	78.0	62.5	1.6	200	800	7	5.20E-02	148.3
SWE2PC_161_NRM	4.165	2069.3	90.4	90.4	54.5	4.9	200	800	7	8.58E-02	82.7
SWE2PC_162_NRM	4.192	2091.9	72.4	72.4	59.8	2.5	200	800	7	3.97E-02	240.9
SWE2PC_163_NRM	4.22	2115.3	98.5	98.5	47.4	5.1	200	800	7	8.93E-02	72.2
SWE2PC_164_NRM	4.246	2132.1	62.6	62.6	65.6	3.2	200	800	7	5.40E-02	152.9
SWE2PC_165_NRM	4.272	2145.7	89.9	89.9	61.2	6.2	200	800	7	8.60E-02	84.7
SWE2PC_166_NRM	4.3	2160.4	89.8	89.8	69.0	3.7	200	800	7	7.27E-02	87.4
SWE2PC_167_NRM	4.327	2174.6	72.4	72.4	66.0	4.6	200	800	7	7.48E-02	76.7
SWE2PC_168_NRM	4.353	2188.3	65.0	65.0	67.0	5.0	200	800	7	5.44E-02	131.9
SWE2PC_169_NRM	4.381	2203	92.4	92.4	60.8	5.6	200	800	7	8.10E-02	82.6
SWE2PC_170_NRM	4.406	2216.1	74.3	74.3	61.6	3.7	200	800	10	8.57E-02	88.2
SWE2PC_171_NRM	4.433	2230.3	65.2	65.2	55.6	1.7	200	800	7	5.00E-02	253.1
SWE2PC_172_NRM	4.46	2244.5	65.2	65.2	54.5	5.2	200	800	7	8.16E-02	80.5
SWE2PC_173_NRM	4.487	2258.7	54.5	54.5	64.3	2.8	200	800	7	6.31E-02	161.2
SWE2PC_174_NRM	4.513	2272.3	35.3	35.3	66.1	1.7	200	800	7	3.94E-02	301.8
SWE2PC_175_NRM	4.54	2286.5	51.3	51.3	68.6	5.6	200	800	7	8.19E-02	76.6
SWE2PC_176_NRM	4.566	2300.2	49.6	49.6	64.2	3.3	200	800	7	4.09E-02	248.7
SWE2PC_177_NRM	4.594	2314.9	54.6	54.6	64.0	3.1	200	800	7	5.61E-02	177.0
SWE2PC_178_NRM	4.621	2329.1	61.8	61.8	70.6	2.8	200	800	7	6.04E-02	81.7
SWE2PC_179_NRM	4.65	2344.3	53.2	53.2	61.0	5.3	200	800	7	6.64E-02	82.3
SWE2PC_180_NRM	4.675	2357.4	48.8	48.8	65.0	5.2	200	800	7	7.28E-02	92.1
SWE2PC_181_NRM	4.702	2371.6	51.8	51.8	65.4	3.0	200	800	7	3.23E-02	257.8
SWE2PC_182_NRM	4.73	2386.3	78.2	78.2	63.2	6.1	200	800	7	9.71E-02	77.5
SWE2PC_183_NRM	4.755	2399.4	47.3	47.3	65.6	3.8	200	800	7	4.35E-02	190.3
SWE2PC_184_NRM	4.782	2413.6	32.0	32.0	61.2	3.1	200	800	7	3.35E-02	334.3
SWE2PC_185_NRM	4.809	2427.8	30.1	30.1	70.4	4.4	200	800	7	6.82E-02	96.8
SWE2PC_186_NRM	4.835	2441.5	16.6	16.6	64.4	2.4	200	800	7	3.46E-02	319.4
SWE2PC_187_NRM	4.863	2456.2	27.9	27.9	60.9	3.0	200	800	7	3.28E-02	297.6
SWE2PC_188_NRM	4.89	2470.4	33.1	33.1	62.5	3.6	200	800	7	5.77E-02	179.6
SWE2PC_189_NRM	4.916	2484	26.4	26.4	61.3	3.5	200	800	7	3.30E-02	296.4
SWE2PC_190_NRM	4.941	2497.1	32.7	32.7	61.2	4.5	200	800	10	7.01E-02	84.9
SWE2PC_191_NRM	4.97	2512.4	9.5	9.5	67.6	2.7	200	800	7	4.30E-02	237.7
SWE2PC_192_NRM	4.994	2525	13.1	13.1	59.3	2.5	200	800	7	2.31E-02	307.9
SWE2PC_193_NRM	5.022	2539.7	11.0	11.0	63.5	4.7	200	800	7	5.86E-02	77.8
SWE2PC_194_NRM	5.048	2553.3	5.7	5.7	57.6	2.6	200	800	7	3.46E-02	289.6
SWE2PC_195_NRM	5.076	2568.1	15.9	15.9	61.9	2.5	200	800	7	1.95E-02	301.2
SWE2PC_196_NRM	5.102	2581.7	26.2	26.2	61.2	3.6	200	800	7	4.75E-02	94.1
SWE2PC_197_NRM	5.129	2595.9	30.5	30.5	66.3	4.4	200	800	7	2.73E-02	281.4
SWE2PC_198_NRM	5.156	2610.1	16.2	16.2	60.7	3.6	200	800	7	4.18E-02	119.1
SWE2PC_199_NRM	5.183	2624.3	356.5	-3.5	70.0	4.1	200	800	7	4.92E-02	190.7
SWE2PC_200_NRM	5.21	2638.4	32.1	32.1	75.4	2.0	200	800	7	3.22E-02	292.2
SWE2PC_201_NRM	5.237	2652.6	28.1	28.1	76.1	3.8	200	800	7	6.65E-02	71.4
SWE2PC_202_NRM	5.263	2666.3	20.2	20.2	73.2	2.5	200	800	7	3.95E-02	202.4
SWE2PC_203_NRM	5.291	2681	48.0	48.0	71.8	4.6	200	800	7	6.27E-02	73.3
SWE2PC_204_NRM	5.319	2695.7	9.2	9.2	67.8	3.0	200	800	7	2.54E-02	298.0
SWE2PC_205_NRM	5.345	2709.4	10.1	10.1	72.2	4.9	200	800	7	4.06E-02	99.2
SWE2PC_206_NRM	5.374	2724.6	21.6	21.6	74.2	2.6	200	800	7	3.99E-02	163.4
SWE2PC_207_NRM	5.401	2738.8	47.0	47.0	71.7	7.6	200	800	7	7.31E-02	69.0
SWE2PC_208_NRM	5.43	2754	79.1	79.1	81.6	4.7	200	800	7	7.63E-02	64.0
SWE2PC_209_NRM	5.456	2766.6	48.0	48.0	75.0	4.8	200	800	7	3.35E-02	87.6
SWE2PC_210_NRM	5.471	2773.8	28.0	28.0	79.5	2.7	200	800	10	4.07E-02	166.0
SWE2PC_211_NRM	5.496	2785.9	61.9	61.9	86.4	4.6	200	800	7	6.31E-02	57.0
SWE2PC_212_NRM	5.521	2797.9	12.8	12.8	79.3	2.6	200	800	7	2.64E-02	243.5

SWE2PC_213_NRM	5.546	2810	171.8	171.8	85.5	5.7	200	800	7	6.79E-02	63.9
SWE2PC_214_NRM	5.571	2822.1	2.1	2.1	82.0	3.4	200	800	7	3.25E-02	157.4
SWE2PC_215_NRM	5.596	2834.1	351.0	-9.0	78.7	3.9	200	800	7	2.55E-02	105.7
SWE2PC_216_NRM	5.621	2846.2	66.6	66.6	80.9	6.1	200	800	7	6.16E-02	60.2
SWE2PC_217_NRM	5.646	2858.3	23.1	23.1	79.1	3.9	200	800	7	2.85E-02	157.8
SWE2PC_218_NRM	5.671	2870.3	24.5	24.5	86.8	9.9	200	800	7	5.57E-02	57.9
SWE2PC_219_NRM	5.696	2882.4	114.2	114.2	79.1	11.3	200	800	7	5.61E-02	49.8
SWE2PC_220_NRM	5.721	2894.5	46.0	46.0	70.4	6.9	200	800	7	3.84E-02	48.8
SWE2PC_221_NRM	5.746	2906.5	38.3	38.3	72.9	7.7	200	800	7	1.93E-02	216.2
SWE2PC_222_NRM	5.771	2918.6	86.5	86.5	69.6	8.4	200	800	7	8.61E-02	55.7
SWE2PC_223_NRM	5.796	2930.7	84.6	84.6	81.9	10.4	200	800	7	5.02E-02	52.4
SWE2PC_224_NRM	5.821	2942.7	33.6	33.6	72.2	6.8	200	800	7	6.74E-02	56.1
SWE2PC_225_NRM	5.846	2954.8	84.4	84.4	65.1	12.0	200	800	7	6.43E-02	50.9
SWE2PC_228_NRM	5.921	2991.4	302.4	-57.6	83.8	9.2	200	800	7	6.10E-02	49.4
SWE2PC_229_NRM	5.946	3003.7	30.7	30.7	85.4	5.7	200	800	7	6.14E-02	62.4
SWE2PC_230_NRM	5.971	3016	8.7	8.7	76.1	6.4	200	800	10	2.81E-02	244.9
SWE2PC_231_NRM	5.996	3028.3	19.6	19.6	79.1	8.6	200	800	7	6.20E-02	56.9
SWE2PC_232_NRM	6.021	3040.6	21.6	21.6	61.8	4.0	200	800	7	3.93E-02	90.2
SWE2PC_233_NRM	6.046	3052.8	3.1	3.1	61.6	5.6	200	800	7	3.15E-02	183.2
SWE2PC_234_NRM	6.071	3065.1	58.8	58.8	50.9	4.9	200	800	7	3.56E-02	101.2
SWE2PC_235_NRM	6.096	3077.4	84.6	84.6	68.8	8.3	200	800	7	7.77E-02	68.1
SWE2PC_236_NRM	6.121	3089.7	40.5	40.5	75.3	6.1	200	800	7	5.57E-02	115.9
SWE2PC_237_NRM	6.146	3102	26.2	26.2	73.6	4.6	200	800	7	2.73E-02	269.6
SWE2PC_238_NRM	6.171	3114.3	52.8	52.8	81.6	2.0	200	800	7	5.77E-02	188.0
SWE2PC_239_NRM	6.196	3126.5	54.6	54.6	80.3	4.7	200	800	7	8.31E-02	104.2
SWE2PC_240_NRM	6.221	3138.8	29.1	29.1	74.7	2.6	200	800	7	3.52E-02	258.4
SWE2PC_241_NRM	6.246	3151.1	33.7	33.7	73.7	2.0	200	800	7	5.10E-02	225.6
SWE2PC_242_NRM	6.271	3163.4	9.6	9.6	70.7	2.8	200	800	7	4.59E-02	306.8
SWE2PC_243_NRM	6.296	3175.7	43.1	43.1	75.2	2.2	200	800	7	9.25E-02	179.7
SWE2PC_244_NRM	6.321	3187.9	6.8	6.8	74.1	4.6	200	800	7	5.83E-02	241.9
SWE2PC_245_NRM	6.346	3200.2	25.2	25.2	73.0	1.9	200	800	7	4.55E-02	307.4
SWE2PC_246_NRM	6.371	3212.5	32.6	32.6	77.1	2.3	200	800	7	9.98E-02	230.9
SWE2PC_247_NRM	6.396	3224.8	18.8	18.8	73.0	1.7	200	800	7	7.67E-02	279.2
SWE2PC_248_NRM	6.421	3237.1	35.7	35.7	73.7	3.3	200	800	7	7.97E-02	243.2
SWE2PC_249_NRM	6.446	3249.3	31.3	31.3	75.6	3.4	200	800	7	1.17E-01	198.7
SWE2PC_250_NRM	6.471	3261.8	17.7	17.7	74.2	2.1	200	800	10	9.20E-02	269.9
SWE2PC_251_NRM	6.496	3275	38.5	38.5	69.7	3.7	200	800	7	6.85E-02	280.4
SWE2PC_252_NRM	6.521	3288.2	10.0	10.0	71.2	1.6	200	800	7	1.08E-01	294.4
SWE2PC_253_NRM	6.546	3301.3	31.2	31.2	71.4	1.4	200	800	7	1.24E-01	286.3
SWE2PC_254_NRM	6.571	3314.5	22.4	22.4	70.7	1.4	200	800	7	1.09E-01	331.5
SWE2PC_255_NRM	6.596	3327.7	14.9	14.9	75.1	2.5	200	800	7	1.40E-01	256.3
SWE2PC_256_NRM	6.621	3340.8	16.1	16.1	72.7	0.7	200	800	7	1.03E-01	318.8
SWE2PC_257_NRM	6.646	3354	1.0	1.0	70.1	2.2	200	800	7	7.60E-02	336.4
SWE2PC_258_NRM	6.671	3367.2	29.4	29.4	71.9	2.0	200	800	7	7.79E-02	319.6
SWE2PC_259_NRM	6.696	3380.3	23.8	23.8	78.0	2.0	200	800	7	1.09E-01	187.9
SWE2PC_260_NRM	6.721	3393.5	358.3	-1.7	75.7	1.7	200	800	7	7.44E-02	308.4
SWE2PC_261_NRM	6.751	3409.3	288.5	-71.5	75.9	2.0	200	800	7	1.48E-01	175.7
SWE2PC_262_NRM	6.776	3422.4	246.4	-113.6	72.9	3.3	200	800	7	1.30E-01	138.2
SWE2PC_263_NRM	6.801	3435.6	243.6	-116.4	80.7	2.9	200	800	7	1.60E-01	138.6
SWE2PC_264_NRM	6.826	3448.8	285.8	-74.2	78.8	4.3	200	800	7	1.04E-01	299.7
SWE2PC_265_NRM	6.851	3461.9	245.1	-114.9	81.3	2.7	200	800	7	1.80E-01	175.3
SWE2PC_266_NRM	6.876	3475.1	318.6	-41.4	86.0	1.7	200	800	7	1.57E-01	215.2
SWE2PC_267_NRM	6.901	3488.3	299.9	-60.1	79.1	1.2	200	800	7	9.81E-02	287.5
SWE2PC_268_NRM	6.926	3501.4	287.1	-72.9	87.9	2.9	200	800	7	1.67E-01	162.2
SWE2PC_269_NRM	6.951	3514.6	270.5	-89.5	82.2	3.2	200	800	7	1.58E-01	153.8
SWE2PC_270_NRM	6.976	3527.8	308.7	-51.3	78.2	1.7	200	800	10	1.11E-01	259.5
SWE2PC_271_NRM	7.001	3543.2	225.8	-134.2	79.3	3.7	200	800	7	1.95E-01	118.9
SWE2PC_272_NRM	7.026	3558.6	234.5	-125.5	80.1	4.4	200	800	7	1.86E-01	125.7
SWE2PC_273_NRM	7.051	3574	256.1	-103.9	80.3	1.2	200	800	7	1.82E-01	181.4
SWE2PC_274_NRM	7.076	3589.3	281.9	-78.1	77.0	2.4	200	800	7	1.24E-01	189.2
SWE2PC_275_NRM	7.101	3604.7	249.3	-110.7	77.9	3.0	200	800	7	1.97E-01	138.9
SWE2PC_276_NRM	7.126	3620.1	244.6	-115.4	73.7	1.3	200	800	7	1.12E-01	174.1
SWE2PC_277_NRM	7.151	3635.4	234.9	-125.1	79.6	3.9	200	800	7	1.91E-01	125.3
SWE2PC_278_NRM	7.176	3650.8	256.8	-103.2	78.3	1.3	200	800	7	1.43E-01	245.2
SWE2PC_279_NRM	7.201	3666.2	270.3	-89.7	77.4	1.9	200	800	7	1.36E-01	263.0
SWE2PC_280_NRM	7.226	3681.5	273.9	-86.1	78.2	2.1	200	800	7	1.61E-01	214.7
SWE2PC_281_NRM	7.251	3696.9	257.0	-103.0	75.3	3.1	200	800	7	1.72E-01	191.9
SWE2PC_282_NRM	7.276	3712.3	289.3	-70.7	76.0	1.3	200	800	7	8.84E-02	251.1
SWE2PC_283_NRM	7.301	3727.7	226.4	-133.6	79.1	3.2	200	800	7	1.43E-01	151.3

SWE2PC_284_NRM	7.326	3743	280.9	-79.1	72.7	1.3	200	800	7	1.17E-01	266.9
SWE2PC_285_NRM	7.351	3758.4	269.9	-90.1	74.3	1.4	200	800	7	1.04E-01	306.0
SWE2PC_286_NRM	7.376	3773.8	277.0	-83.0	77.2	2.2	200	800	7	1.36E-01	194.0
SWE2PC_287_NRM	7.401	3789.1	312.2	-47.8	86.4	2.2	200	800	7	1.49E-01	177.3
SWE2PC_288_NRM	7.426	3804.5	263.7	-96.3	76.3	2.6	200	800	7	1.21E-01	188.1
SWE2PC_289_NRM	7.451	3819.9	297.3	-62.7	77.5	1.3	200	800	7	1.31E-01	277.5
SWE2PC_290_NRM	7.476	3835.2	309.1	-50.9	72.9	1.1	200	800	10	1.13E-01	314.3
SWE2PC_291_NRM	7.501	3850.6	272.5	-87.5	81.0	2.1	200	800	7	1.34E-01	182.9
SWE2PC_292_NRM	7.526	3866	317.6	-42.4	58.7	1.7	200	800	7	5.98E-02	288.8
SWE2PC_293_NRM	7.551	3881.4	342.0	-18.0	72.0	1.3	200	800	7	7.01E-02	270.2
SWE2PC_294_NRM	7.576	3896.7	291.7	-68.3	66.2	3.6	200	800	7	1.14E-01	164.9
SWE2PC_295_NRM	7.601	3912.1	273.3	-86.7	72.7	3.9	200	800	7	1.38E-01	143.3
SWE2PC_296_NRM	7.626	3925.6	276.8	-83.2	72.5	1.7	200	800	7	8.27E-02	266.7
SWE2PC_297_NRM	7.651	3938.8	248.2	-111.8	81.9	2.9	200	800	7	1.30E-01	109.9
SWE2PC_298_NRM	7.676	3951.9	268.5	-91.5	75.4	1.5	200	800	7	8.93E-02	222.7
SWE2PC_299_NRM	7.701	3965.1	288.9	-71.1	66.3	2.1	200	800	7	7.63E-02	310.5
SWE2PC_300_NRM	7.726	3978.2	283.5	-76.5	70.5	2.0	200	800	7	1.17E-01	225.5
SWE2PC_301_NRM	7.751	3991.4	285.6	-74.4	73.3	1.6	200	800	7	7.93E-02	286.1
SWE2PC_302_NRM	7.776	4004.6	293.6	-66.4	73.1	2.8	200	800	7	1.37E-01	222.8
SWE2PC_303_NRM	7.801	4017.7	305.0	-55.0	71.0	1.4	200	800	7	9.14E-02	302.6
SWE2PC_304_NRM	7.826	4030.9	281.3	-78.7	73.9	2.6	200	800	7	1.49E-01	215.9
SWE2PC_305_NRM	7.851	4044	285.1	-74.9	68.2	1.4	200	800	7	1.34E-01	307.5
SWE2PC_306_NRM	7.876	4057.2	293.4	-66.6	71.8	1.3	200	800	7	1.24E-01	354.1
SWE2PC_307_NRM	7.901	4070.4	294.7	-65.3	71.5	1.3	200	800	7	1.69E-01	272.2
SWE2PC_308_NRM	7.926	4083.5	300.7	-59.3	69.5	1.0	200	800	7	1.47E-01	331.7
SWE2PC_309_NRM	7.951	4096.7	299.9	-60.1	69.5	1.6	200	800	7	1.80E-01	289.4
SWE2PC_310_NRM	7.976	4109.8	304.4	-55.6	69.3	1.1	200	800	10	1.48E-01	324.7
SWE2PC_311_NRM	8.001	4123	289.8	-70.2	68.6	1.0	200	800	7	1.87E-01	367.9
SWE2PC_312_NRM	8.026	4136.2	314.1	-45.9	63.9	1.9	200	800	7	1.65E-01	357.0
SWE2PC_313_NRM	8.051	4149.3	312.0	-48.0	67.5	0.8	200	800	7	1.45E-01	376.3
SWE2PC_314_NRM	8.076	4162.5	310.3	-49.7	75.7	2.3	200	800	7	1.86E-01	287.9
SWE2PC_315_NRM	8.101	4175.6	296.9	-63.1	68.9	3.3	200	800	7	1.49E-01	352.1
SWE2PC_316_NRM	8.126	4188.8	304.9	-55.1	65.3	1.6	200	800	7	1.62E-01	368.9
SWE2PC_317_NRM	8.151	4202	307.3	-52.7	68.1	2.3	200	800	7	1.86E-01	288.8
SWE2PC_318_NRM	8.176	4215.1	302.9	-57.1	68.9	1.4	200	800	7	1.59E-01	321.3
SWE2PC_319_NRM	8.201	4228.3	312.8	-47.2	74.0	2.5	200	800	7	1.85E-01	266.4
SWE2PC_320_NRM	8.226	4241.4	305.3	-54.7	72.1	1.8	200	800	7	1.75E-01	286.6